

Testing LRD in the spectral domain for functional time series in manifolds

M.D. Ruiz-Medina¹, R.M. Crujeiras²

¹ Department of Statistics and Operation Research, University of Granada

² Galician Center for Mathematical Research and Technology, CITMAga, Universidad de Santiago de Compostela

Abstract

A statistical hypothesis test for long range dependence (LRD) in manifold-supported functional time series is formulated in the spectral domain. The proposed test statistic is based on the weighted periodogram operator, assuming that the elements of the spectral density operator family are invariant with respect to the group of isometries of the manifold. A Central Limit Theorem is derived to obtain the asymptotic Gaussian distribution of the proposed test statistics operator under the null hypothesis. The rate of convergence to zero, in the Hilbert–Schmidt operator norm, of the bias of the integrated empirical second and fourth order cumulant spectral density operators is established under the alternative hypothesis. The consistency of the test is then derived, from the obtained consistency of the integrated weighted periodogram operator under LRD. Practical implementation of our testing approach is based on the random projection methodology. The frequency-varying Karhunen–Loève expansion of invariant Gaussian random spectral Hilbert–Schmidt kernels on manifolds is considered for generation of random directions in the implementation of this methodology. A simulation study illustrates the main results regarding asymptotic normality and consistency, and the empirical size and power properties of the proposed testing approach.

Keywords Asymptotic normality, bias, compact manifolds, consistency, empirical cumulant spectral density operator, functional time series, integrated weighted periodogram operator, long-range dependence, spectral density operator.

1 Introduction

Spherical functional time series analysis helps in understanding the dynamics and spatiotemporal patterns of data that are embedded into the sphere, providing valuable insights for prediction, monitoring, and decision-making. Time series analysis of global temperature data distribution among other climate variables, usually arising in Climate Science and Meteorology, can be performed in a more efficient way by adopting a functional time series framework (see [33]). That is the case of ocean currents, and other marine functional time series to be analyzed in Oceanography studies (see, e.g., [36]; [38]). Other areas demanding this type of techniques are Geophysics, Astronomy and Astrophysics. In the last few decades, the cosmic microwave background radiation variation analysis over time has gained special attention (see [11]; [18]; [19]). In a more general manifold setting, functional time series analysis is often applied in Medical Imaging, Computer Vision and Graphics (see [37]; [39]; [41], among others). This paper focuses on the spectral analysis of manifold-supported functional time series, paying special attention to LRD analysis.

The spectral analysis of functional time series has mainly been developed under Short Range Dependence (SRD). In this context, based on the weighted periodogram operator, a nonparametric framework is adopted in [24]. Particularly, the asymptotic normality of the functional discrete Fourier transform (fDFT), and the weighted periodogram operator of the curve data are proved under suitable summability conditions on the cumulant spectral density operators. The consistency of the weighted periodogram operator, in the sense of the integrated mean square error, as well as pointwise, in the Hilbert–Schmidt operator norm, is also derived under SRD. In [25], a harmonic principal component analysis of functional time series in the temporal functional spectral domain is derived, based on a Karhunen–Loève-like decomposition, the so-called Cramér–Karhunen–Loève representation (see also [31]). In the context of functional regression, some applications are presented in [26], [30] and [34]. Hypothesis testing for detecting modelling differences in functional time series dynamics is addressed in [35] in the functional spectral domain.

Only a few contributions can be found on LRD functional time series analysis. One of the key approaches in the current literature is presented in [16], where the eigendecomposition of the long-run covariance operator is considered, under an asymptotic semiparametric functional principal component framework. The consistent estimation of the dimension and the orthonormal functions spanning the dominant subspace, where the projected curve process displays the largest dependence range is derived. Fractionally integrated functional autoregressive moving averages processes constitute an interesting example of this modelling framework.

A first attempt to characterize LRD in functional time series in the spectral domain can be found in [32], adopting the theoretical framework of operator-valued random fields, including fractional Brownian motion with operator-valued Hurst coefficient (see, e.g., [9]; [10]; [20]; [27] and [28]). Specifically, the LRD functional time series setting introduced in [32], in a functional semiparametric framework in the spectral domain, is based on the consideration of a parametrized LRD operator. The eigenvalues of this operator induce different levels of singularity at zero frequency. Thus, different levels of LRD are displayed in time by the process projected into different eigenspaces. The asymptotic unbiasedness in the Hilbert–Schmidt operator norm of the integrated periodogram operator under LRD is proved beyond any structural assumptions. The weak-consistent minimum contrast estimation of the LRD operator is addressed in the spectral domain under a Gaussian scenario. Interesting examples of this setting are analyzed in [22], where the spectral analysis of multifractionally integrated functional time series in manifolds is considered. In particular, multifractionally integrated spherical functional ARMA models (i.e., multifractionally integrated SPHARMA models) are analyzed through simulations. In this modelling framework, SRD and LRD can coexist at different spherical scales.

Up to our knowledge, no further developments have been achieved in the spectral analysis of LRD functional time series. In this paper we perform a weighted periodogram operator based analysis, requiring the asymptotic analysis of the bias of the integrated fourth-order empirical cumulant spectral density operators, to prove consistency of the integrated weighted periodogram operator under LRD. Its application to spectral statistical hypothesis testing of LRD in $L^2(\mathbb{M}_d, d\nu, \mathbb{R})$ -valued correlated sequences constitutes one of the main goals of this work. Here, $L^2(\mathbb{M}_d, d\nu, \mathbb{R})$ denotes the space of real-valued square integrable functions on a Riemannian manifold \mathbb{M}_d , embedded into \mathbb{R}^{d+1} , given by a connected and compact two-point homogeneous space. The topological dimension of \mathbb{M}_d is d , and $d\nu$ denotes the normalized Riemannian measure on \mathbb{M}_d . In what follows, we will consider $X = \{X_t, t \in \mathbb{Z}\}$ to be a functional sequence such that $\mathcal{P}(X_t \in L^2(\mathbb{M}_d, d\nu, \mathbb{R})) = 1$, for every $t \in \mathbb{Z}$, with \mathcal{P} denoting the probability measure defined on the basic probability space $(\Omega, \mathcal{Q}, \mathcal{P})$, i.e., for every $t \in \mathbb{Z}$,

$$X_t : (\Omega, \mathcal{Q}, \mathcal{P}) \longrightarrow L^2(\mathbb{M}_d, d\nu, \mathbb{R}) \quad (1)$$

is a measurable mapping.

The invariance of the elements of the spectral density operator family of X under the group of isometries of the manifold \mathbb{M}_d is assumed along the paper. A frequency-varying eigenvalue sequence then characterizes the pure point spectra of the elements of the spectral density operator family, with respect to the orthonormal basis of eigenfunctions of the Laplace–Beltrami operator. This

invariance assumption is exploited in the derived Central Limit Theorem that characterizes the asymptotic distribution of the proposed test statistics operator under the null hypothesis, which states that X displays SRD. In our formulation of the alternative hypothesis on LRD, we adopt a semiparametric framework in terms of a functional parameter given by the LRD operator. In contrast with the approach presented in [32], here we do not assume a parameterization of the eigenvalues of the LRD operator. The new bias asymptotic LRD functional spectral results are obtained under this scenario. Specifically, the second and fourth order functional spectral bias asymptotics analysis under LRD is addressed in Lemmas 2 and 3. Proposition 1 shows the divergence, in the Hilbert–Schmidt operator norm, of the mean of the test statistics operator under the alternative hypothesis. Theorem 2 derives suitable conditions, in particular, on the nonparametric functional spectral factor, to ensure consistency of the integrated weighted periodogram operator under LRD. Theorem 3 then provides the almost surely divergence of the test statistics in the Hilbert–Schmidt operator norm under the alternative, yielding the consistency of the test.

Theorem 3 also plays a crucial role in the implementation in practice of the proposed testing procedure, based on rejecting the null hypothesis when the random Fourier coefficients of the test operator statistics, suitably standardized according to Theorem 1, cross an upper or lower tail standard normal critical value. The orthonormal basis involved in the computation of these coefficients is constructed by the tensor product of the eigenfunctions of the Laplace Beltrami operator. The random projection methodology (see Theorem 4.1 in [5]) can be implemented here to alleviate the dimensionality problem. Specifically, when the moments of our test statistics operator satisfy the Carleman condition, our testing procedure is equivalent to rejecting the null hypothesis when the absolute value of a random projection of the test statistics is larger than an upper tail standard normal critical value. In the implementation of the random projection methodology, the Karhunen–Loève expansion in Lemma 4 below can be considered for generation of the involved Gaussian random directions. Furthermore, as illustrated in the simulation study undertaken, the empirical size properties of the proposed testing procedure are quite robust, and competitive in terms of power (see Section 5.4).

The outline of the paper is now described. In Section 1.1, the functional spectral background material is introduced. Our hypothesis testing procedure is formulated in a functional semiparametric spectral framework in Section 1.2. The asymptotic Gaussian distribution of the test statistics operator under the null hypothesis H_0 is obtained in Theorem 1 in Section 2. Asymptotics of the bias of the integrated second and fourth order empirical cumulant spectral density operators under LRD are derived in Section 3. Section 4 provides the preliminary results required for consistency of the test, which is derived in Theorem 3 of this

section. Practical implementation is also discussed in this section. In Section 5.1, a simulation study is undertaken to illustrate the asymptotic Gaussian distribution of the proposed test statistics operator under the null hypothesis, in the context of spherical functional time series. The consistency of the test is also illustrated in Section 5.2, in the framework of multifractionally integrated spherical functional time series. This numerical analysis is extended in Section 5.3 to a wider family of LRD operators allowing stronger persistency in time, displayed by the projected process in the dominant subspace. Section 5.4 analyzes empirical size and power properties of the proposed test. Section 6 summarizes conclusions of the simulation study, focusing on the large functional sample size properties of the proposed test statistics operator under different bandwidth parameter scenarios, from additional numerical results. The proofs of the results of this paper can be found in the Appendices. These Appendices also provide the figures illustrating Examples 1–4 in Sections 5.2–5.3.

1.1 Background

Along this work we will assume that $X = \{X_t, t \in \mathbb{Z}\}$ in (1) is a stationary zero-mean functional sequence, and that its family of nuclear covariance operators $\{\mathcal{R}_\tau, \tau \in \mathbb{Z}\}$ satisfies $\mathcal{R}_\tau = E[X_s \otimes X_{s+\tau}] = E[X_{s+\tau} \otimes X_s]$, for every $s, \tau \in \mathbb{Z}$. The elements of this family are characterized in the spectral domain by the spectral density operator family $\{\mathcal{F}_\omega, \omega \in [-\pi, \pi]\}$. The assumed invariance of the elements of these families with respect to the group of isometries of \mathbb{M}_d yields to their diagonal series expansion in terms of $\{S_{n,j}^d \otimes \overline{S_{n,j}^d}, j = 1, \dots, \Gamma(n, d), n \in \mathbb{N}_0\}$, with $\{S_{n,j}^d, j = 1, \dots, \Gamma(n, d), n \in \mathbb{N}_0\}$ being the orthonormal basis of eigenfunctions of the Laplace–Beltrami operator Δ_d on $L^2(\mathbb{M}_d, d\nu, \mathbb{C})$ (see, e.g., [13]; [14]). In particular,

$$\begin{aligned} \mathcal{F}_\omega & \underset{\mathcal{S}(L^2(\mathbb{M}_d, d\nu; \mathbb{C}))}{=} \frac{1}{2\pi} \sum_{\tau \in \mathbb{Z}} \exp(-i\omega\tau) \mathcal{R}_\tau \\ & \underset{\mathcal{S}(L^2(\mathbb{M}_d, d\nu; \mathbb{C}))}{=} \sum_{n \in \mathbb{N}_0} f_n(\omega) \sum_{j=1}^{\Gamma(n, d)} S_{n,j}^d \otimes \overline{S_{n,j}^d}, \quad \omega \in [-\pi, \pi], \end{aligned} \quad (2)$$

where, for every $n \in \mathbb{N}_0$, $\Gamma(n, d)$ denotes the dimension of the eigenspace \mathcal{H}_n associated with the eigenvalue $\lambda_n(\Delta_d)$ of the Laplace Beltrami operator Δ_d (see, e.g., Section 2.1 in [17]). The equality $\underset{\mathcal{S}(L^2(\mathbb{M}_d, d\nu; \mathbb{C}))}{=}$ means identity in the norm of the space of Hilbert–Schmidt operators on $L^2(\mathbb{M}_d, d\nu; \mathbb{C})$, the space of complex-valued square integrable functions on \mathbb{M}_d . Specifically, the equality in (2) means

that

$$\int_{\mathbb{M}_d \times \mathbb{M}_d} \left| f_\omega(x, y) - \sum_{n=0}^{\infty} f_n(\omega) \sum_{j=1}^{\Gamma(n,d)} S_{n,j}^d(x) \overline{S_{n,j}^d(y)} \right|^2 d\nu(x) d\nu(y) = 0,$$

where f_ω is the kernel of the integral operator \mathcal{F}_ω , for every $\omega \in [-\pi, \pi]$.

Let $\{X_t, t = 0, \dots, T-1\}$ be a functional sample of size $T \geq 2$ of X . The fDFT $\tilde{X}_\omega^{(T)}$ is defined as

$$\tilde{X}_\omega^{(T)}(x) = \frac{1}{\sqrt{2\pi T}} \sum_{t=0}^{T-1} X_t(x) \exp(-i\omega t), \quad x \in \mathbb{M}_d, \quad \omega \in [-\pi, \pi]. \quad (3)$$

The kernel $p_\omega^{(T)}$ of the periodogram operator $\mathcal{P}_\omega^{(T)} = \tilde{X}_\omega^{(T)} \otimes \tilde{X}_{-\omega}^{(T)}$ satisfies, for $\omega \in [-\pi, \pi]$,

$$p_\omega^{(T)}(x, y) = \frac{1}{2\pi T} \sum_{t=0}^{T-1} \sum_{s=0}^{T-1} X_t(x) X_s(y) \exp(-i\omega(t-s)), \quad \forall x, y \in \mathbb{M}_d. \quad (4)$$

We will denote by $f_\omega^{(T)}(x, y) = \text{cum}(\tilde{X}_\omega^{(T)}(x), \tilde{X}_{-\omega}^{(T)}(y)) = E[p_\omega^{(T)}(x, y)]$, $x, y \in \mathbb{M}_d$, the kernel of the cumulant operator $\mathcal{F}_\omega^{(T)}$ of order 2 of the fDFT $\tilde{X}_\omega^{(T)}$ over the diagonal $\omega \in [-\pi, \pi]$. Note that, for $\omega \in [-\pi, \pi]$, and $T \geq 2$, the Féjer kernel is given by

$$F_T(\omega) = \frac{1}{T} \sum_{t=1}^T \sum_{s=1}^T \exp(-i(t-s)\omega) = \frac{1}{T} \left[\frac{\sin(T\omega/2)}{\sin(\omega/2)} \right]^2. \quad (5)$$

The weighted periodogram operator, denoted as $\hat{\mathcal{F}}_\omega^{(T)}$, has kernel $\hat{f}_\omega^{(T)}(x, y)$ given by,

$$\hat{f}_\omega^{(T)}(x, y) = \left[\frac{2\pi}{T} \right] \sum_{s=1}^{T-1} W^{(T)} \left(\omega - \frac{2\pi s}{T} \right) p_{\frac{2\pi s}{T}}^{(T)}(x, y), \quad x, y \in \mathbb{M}_d, \quad \omega \in [-\pi, \pi], \quad (6)$$

where $W^{(T)}$ is a weight function satisfying

$$W^{(T)}(x) = \sum_{j \in \mathbb{Z}} \frac{1}{B_T} W \left(\frac{x + 2\pi j}{B_T} \right), \quad (7)$$

with B_T being the positive bandwidth parameter. Function W is a real-valued function defined on \mathbb{R} such that W is positive, even, and bounded in variation; $W(x) = 0$, if $|x| \geq 1$; $\int_{\mathbb{R}} |W(x)|^2 dx < \infty$; $\int_{\mathbb{R}} W(x) dx = 1$.

1.2 Hypothesis testing

The elements involved, and the conditions assumed in the functional spectral domain, characterizing the SRD and LRD scenarios respectively tested under the null H_0 and the alternative H_1 hypotheses, are now introduced. The proposed test statistics operator based on the weighted periodogram operator is also formulated.

Stationary SRD functional time series are characterized by the summability of the series of trace norms of the elements of the family of covariance operators $\{\mathcal{R}_\tau, \tau \in \mathbb{Z}\}$ (see, e.g., [24]). That is, X displays SRD if and only if $\sum_{\tau \in \mathbb{Z}} \|\mathcal{R}_\tau\|_{L^1(L^2(\mathbb{M}_d, d\nu, \mathbb{R}))} < \infty$, where $L^1(L^2(\mathbb{M}_d, d\nu, \mathbb{R}))$ denotes the space of trace operators on $L^2(\mathbb{M}_d, d\nu, \mathbb{R})$. In our setting, this condition can be formulated as follows:

$$\sum_{\tau \in \mathbb{Z}} \|\mathcal{R}_\tau\|_{L^1(L^2(\mathbb{M}_d, d\nu, \mathbb{R}))} = \sum_{\tau \in \mathbb{Z}} \sum_{n \in \mathbb{N}_0} \Gamma(n, d) \left| \int_{-\pi}^{\pi} \exp(i\omega\tau) f_n(\omega) d\omega \right| < \infty. \quad (8)$$

When (8) fails, X is said to display LRD. In what follows, we will adopt the LRD scenario introduced in [32], given by

$$\mathcal{F}_\omega = \mathcal{M}_\omega |\omega|^{-\mathcal{A}}, \quad \omega \in [-\pi, \pi], \quad (9)$$

where the invariant positive self-adjoint operators \mathcal{M}_ω and $|\omega|^{-\mathcal{A}}$ are composed yielding the definition of \mathcal{F}_ω . Specifically, \mathcal{A} denotes the LRD operator on $L^2(\mathbb{M}_d, d\nu; \mathbb{C})$. Operator $|\omega|^{-\mathcal{A}}$ in (9) is interpreted as in [4], [27] and [28], where \mathcal{A} plays the role of operator-valued Hurst coefficient in the setting of fractional Brownian motion introduced in this framework. Moreover, \mathcal{M}_ω is the regular spectral operator reflecting markovianess when the null space of \mathcal{A} coincides with $L^2(\mathbb{M}_d, d\nu; \mathbb{C})$. Thus,

$$\sum_{\tau \in \mathbb{Z}} \left\| \int_{[-\pi, \pi]} \exp(i\omega\tau) \mathcal{M}_\omega d\omega \right\|_{L^1(L^2(\mathbb{M}_d, d\nu, \mathbb{R}))} < \infty, \quad (10)$$

where the operator integrals are understood as improper operator Stieltjes integrals which converge strongly (see, e.g., Section 8.2.1 in [29]).

We will apply the spectral theory of self-adjoint operators (see, e.g., [8]) in terms of the common spectral kernel

$$\Upsilon(x, y) = \sum_{n \in \mathbb{N}_0} \sum_{j=1}^{\Gamma(n, d)} S_{n,j}^d(x) \overline{S_{n,j}^d(y)}, \quad x, y \in \mathbb{M}_d,$$

under the assumed invariance property with respect to the group of isometries of \mathbb{M}_d .

The point spectrum of \mathcal{A} is given by $\{\alpha(n), n \in \mathbb{N}_0\}$, with $l_\alpha \leq \alpha(n) \leq L_\alpha$, for every $n \in \mathbb{N}_0$, and $l_\alpha, L_\alpha \in (0, 1/2)$. It is assumed that LRD operator \mathcal{A} has kernel $\mathcal{K}_{\mathcal{A}}$ admitting the following series expansion in the weak-sense:

$$\mathcal{K}_{\mathcal{A}}(x, y) = \sum_{n \in \mathbb{N}_0} \alpha(n) \sum_{j=1}^{\Gamma(n, d)} S_{n, j}^d \otimes \overline{S_{n, j}^d}(x, y), \quad x, y \in \mathbb{M}_d. \quad (11)$$

Specifically, identity (11) is understood in the following sense, for every $f, g \in C^\infty(\mathbb{M}_d)$, the space of infinitely differentiable functions with compact support in \mathbb{M}_d ,

$$\mathcal{A}(f)(g) = \int_{\mathbb{M}_d \times \mathbb{M}_d} f(x)g(y) \sum_{n \in \mathbb{N}_0} \alpha(n) \sum_{j=1}^{\Gamma(n, d)} S_{n, j}^d(x) \overline{S_{n, j}^d}(y) d\nu(x) d\nu(y). \quad (12)$$

Note that, under the conditions assumed, \mathcal{A} and \mathcal{A}^{-1} are bounded, and $\|\mathcal{A}\|_{\mathcal{L}(L^2(\mathbb{M}_d, d\nu, \mathbb{C}))} < 1/2$, with $\|\cdot\|_{\mathcal{L}(L^2(\mathbb{M}_d, d\nu, \mathbb{C}))}$ denoting the norm in the space $\mathcal{L}(L^2(\mathbb{M}_d, d\nu, \mathbb{C}))$ of bounded linear operators on $L^2(\mathbb{M}_d, d\nu, \mathbb{C})$.

In a similar way, operator $|\omega|^{-\mathcal{A}}$ is interpreted as

$$|\omega|^{-\mathcal{A}}(f)(g) = \int_{\mathbb{M}_d \times \mathbb{M}_d} f(x)g(y) \sum_{n \in \mathbb{N}_0} \frac{1}{|\omega|^{\alpha(n)}} \sum_{j=1}^{\Gamma(n, d)} S_{n, j}^d \otimes \overline{S_{n, j}^d}(x, y), d\nu(x) d\nu(y), \quad (13)$$

for every $f, g \in C^\infty(\mathbb{M}_d)$ and $\omega \in [-\pi, \pi] \setminus \{0\}$.

Operator \mathcal{M}_ω in (9) is a Hilbert–Schmidt operator on $L^2(\mathbb{M}_d, d\nu; \mathbb{C})$, whose kernel $\mathcal{K}_{\mathcal{M}_\omega}(x, y)$ admits the following series expansion in the norm of the space $\mathcal{S}(L^2(\mathbb{M}_d, d\nu; \mathbb{C}))$:

$$\mathcal{K}_{\mathcal{M}_\omega}(x, y) = \sum_{n \in \mathbb{N}_0} M_n(\omega) \sum_{j=1}^{\Gamma(n, d)} S_{n, j}^d \otimes \overline{S_{n, j}^d}(x, y), \quad x, y \in \mathbb{M}_d, \quad \omega \in [-\pi, \pi], \quad (14)$$

where $\{M_n(\omega), n \in \mathbb{N}_0\}$ denotes the sequence of positive eigenvalues. For each $n \in \mathbb{N}_0$, $M_n(\omega)$, $\omega \in [-\pi, \pi]$, is a continuous positive slowly varying function at $\omega = 0$ in the Zygmund's sense (see Definition 6.6 in [1], and Assumption IV in [32]). Equation (10) can be rewritten, in terms of $\{M_n(\omega), n \in \mathbb{N}_0, \omega \in [-\pi, \pi]\}$, as follows:

$$\sum_{\tau \in \mathbb{Z}} \sum_{n \in \mathbb{N}_0} \Gamma(n, d) \left| \int_{-\pi}^{\pi} \exp(i\omega\tau) M_n(\omega) d\omega \right| < \infty. \quad (15)$$

Equation (15) implies that X displays SRD, when $\alpha(n) = 0$, for every $n \in \mathbb{N}_0$. Under (15), $\{\mathcal{M}_\omega, \omega \in [-\pi, \pi]\}$ is also included in the trace class.

Under the above setting of conditions,

$$\int_{-\pi}^{\pi} \|\mathcal{F}_{\omega}\|_{\mathcal{S}(L^2(\mathbb{M}_d, d\nu, \mathbb{C}))}^2 d\omega < \infty, \quad (16)$$

i.e., $\|\mathcal{F}_{\omega}\|_{\mathcal{S}(L^2(\mathbb{M}_d, d\nu, \mathbb{C}))} \in L^2([-\pi, \pi])$, with $L^2([-\pi, \pi])$ being the space of square integrable functions on the interval $[-\pi, \pi]$. Condition (16) plays a crucial role in the derivation of the results of this paper under LRD.

From equations (9)–(14), the elements of the positive frequency varying eigenvalue sequence $\{f_n(\omega), n \in \mathbb{N}_0\}$ in (2) admit the following expression:

$$f_n(\omega) = \frac{M_n(\omega)}{|\omega|^{\alpha(n)}}, \quad \omega \in [-\pi, \pi], \quad n \in \mathbb{N}_0. \quad (17)$$

Note that, since $\sin(\omega) \sim \omega, \omega \rightarrow 0$,

$$|1 - \exp(-i\omega)|^{-A} = [4 \sin^2(\omega/2)]^{-A/2} \sim |\omega|^{-A}, \quad \omega \rightarrow 0. \quad (18)$$

Sequence (17) is involved in the formulation of the alternative hypothesis H_1 in our proposal for testing SRD against LRD in the spectral domain. Specifically, the following testing problem is considered:

$$H_0 : f_n(\omega) = M_n(\omega), \quad \omega \in [-\pi, \pi], \quad \forall n \in \mathbb{N}_0 \quad (19)$$

$$H_1 : f_n(\omega) = M_n(\omega) |\omega|^{-\alpha(n)}, \quad \omega \in [-\pi, \pi], \quad \forall n \in \mathbb{N}_0. \quad (20)$$

Our main goal is to design a consistent test in the spectral domain. Such a design must capture the singularities at zero frequency at different manifold resolution levels when H_1 in (20) holds. To this aim, our test operator statistic, denoted as \mathcal{S}_{B_T} , is defined under the integral sign as the product of a scaled weighted periodogram operator, and a truncated Dirac Delta distribution depending on the functional sample size. This integral formulation approximates in a suitable way the functional spectral behavior at zero frequency. Specifically,

$$\mathcal{S}_{B_T} = \sqrt{B_T T} \int_{[-\sqrt{B_T}/2, \sqrt{B_T}/2]} \widehat{\mathcal{F}}_{\omega}^{(T)} \frac{d\omega}{\sqrt{B_T}}, \quad (21)$$

where the kernel of the integral operator $\widehat{\mathcal{F}}_{\omega}^{(T)}$ has been introduced in equation (6), with, as before, B_T being the bandwidth parameter. Denote by $\mathbb{I}_{[-\sqrt{B_T}/2, \sqrt{B_T}/2]}$ the indicator function on the interval $[-\sqrt{B_T}/2, \sqrt{B_T}/2]$. Note that $\frac{\mathbb{I}_{[-\sqrt{B_T}/2, \sqrt{B_T}/2]}}{\sqrt{B_T}}$ converges, as $T \rightarrow \infty$, in the weak sense, i.e., in the sense of generalized functions (see [12]), to a Dirac Delta distribution at zero frequency.

2 Preliminary results under SRD

The following lemma will be applied in the proof of the main result of this section, Theorem 1, deriving the asymptotic Gaussian distribution of \mathcal{S}_{B_T} in (21) under H_0 . Specifically, Lemma 1 provides the asymptotic Gaussian distribution of the weighted periodogram operator $\widehat{\mathcal{F}}_\omega^{(T)}$ under H_0 . Its proof can be obtained in the same way as in [24], where this result is established for the separable Hilbert space $H = L^2([0, 1], \mathbb{C})$.

Lemma 1 *Assume that $E\|X_0\|^k < \infty$, for all $k \geq 2$, and*

- (i) $\sum_{t_1, \dots, t_{k-1} \in \mathbb{Z}} \|\text{cum}(X_{t_1}, \dots, X_{t_{k-1}}, X_0)\|_{L^2(\mathbb{M}_d^k, \otimes_{i=1}^k d\nu(x_i), \mathbb{R})} < \infty$, $k \geq 2$
- (i') $\sum_{t_1, \dots, t_{k-1} \in \mathbb{Z}} (1 + |t_j|) \|\text{cum}(X_{t_1}, \dots, X_{t_{k-1}}, X_0)\|_{L^2(\mathbb{M}_d^k, \otimes_{i=1}^k d\nu(x_i), \mathbb{R})} < \infty$,
for $k \in \{2, 4\}$, $j < k$
- (ii) $\sum_{t \in \mathbb{Z}} (1 + |t|) \|\mathcal{R}_t\|_{L^1(L^2(\mathbb{M}_d, d\nu, \mathbb{R}))} < \infty$
- (iii) $\sum_{t_1, t_2, t_3 \in \mathbb{Z}} \|\mathcal{R}_{t_1, t_2, t_3}\|_{L^1(L^2(\mathbb{M}_d^2, \otimes_{i=1}^2 d\nu(x_i), \mathbb{R}))} < \infty$.

Then, for every frequencies ω_j , $j = 1, \dots, J$, with $J < \infty$,

$$\sqrt{B_T T}(\widehat{f}_{\omega_j}^{(T)} - E[\widehat{f}_{\omega_j}^{(T)}]) \rightarrow_D \widehat{f}_{\omega_j}, \quad j = 1, \dots, J \quad (22)$$

where \rightarrow_D denotes the convergence in distribution. Here, \widehat{f}_{ω_j} , $j = 1, \dots, J$, are jointly zero-mean complex Gaussian elements in $\mathcal{S}(L^2(\mathbb{M}_d, d\nu, \mathbb{C})) = L^2(\mathbb{M}_d^2, d\nu \otimes d\nu, \mathbb{C})$, with covariance kernel:

$$\begin{aligned} \text{cov}(\widehat{f}_{\omega_i}(x_1, y_1), \widehat{f}_{\omega_j}(x_2, y_2)) &= 2\pi \|W\|_{L^2(\mathbb{R})}^2 \{ \eta(\omega_i - \omega_j) f_{\omega_i}(x_1, x_2) f_{-\omega_i}(y_1, y_2) \\ &+ \eta(\omega_i + \omega_j) f_{\omega_i}(x_1, y_2) f_{-\omega_i}(y_1, x_2) \}, \quad (x_i, y_i) \in \mathbb{M}_d^2, \quad i = 1, 2, \end{aligned} \quad (23)$$

with $\eta(\omega) = 1$, for $\omega \in 2\pi\mathbb{Z}$, and $\eta(\omega) = 0$, otherwise. Thus, \widehat{f}_{ω_i} and \widehat{f}_{ω_j} are independent for $\omega_i + \omega_j \neq 0, \text{ mod } 2\pi$ and $\omega_i - \omega_j \neq 0, \text{ mod } 2\pi$. For zero frequency modulus 2π the limit Gaussian random element is in $\mathcal{S}(L^2(\mathbb{M}_d, d\nu, \mathbb{R})) = L^2(\mathbb{M}_d^2, d\nu \otimes d\nu, \mathbb{R})$.

Proof. See Theorem 3.7 in [24].

As announced, the next result provides the asymptotic Gaussian distribution of the test statistics operator \mathcal{S}_{B_T} under H_0 . The convergence to a Gaussian random element in the norm of the space $\mathcal{L}_{\mathcal{S}(L^2(\mathbb{M}_d, d\nu, \mathbb{C}))}^2(\Omega, \mathcal{A}, P)$ is also obtained. Here, $\mathcal{L}_{\mathcal{S}(L^2(\mathbb{M}_d, d\nu, \mathbb{C}))}(\Omega, \mathcal{A}, P)$ denotes the space of zero-mean second-order $\mathcal{S}(L^2(\mathbb{M}_d, d\nu, \mathbb{C}))$ -valued random variables with the norm $\sqrt{E\|\cdot\|_{\mathcal{S}(L^2(\mathbb{M}_d, d\nu, \mathbb{C}))}^2}$.

Theorem 1 Under H_0 , assume that the conditions of Lemma 1 hold. Then,

$$\mathcal{S}_{B_T} - E[\mathcal{S}_{B_T}] \rightarrow_D Y_0^{(\infty)}, \quad T \rightarrow \infty, \quad (24)$$

where \mathcal{S}_{B_T} has been introduced in (21), and $Y_0^{(\infty)}$ is a zero-mean Gaussian random element in $\mathcal{S}(L^2(\mathbb{M}_d, d\nu, \mathbb{R}))$, whose autocovariance operator $\mathcal{R}_{Y_0^{(\infty)}} = E[Y_0^{(\infty)} \otimes Y_0^{(\infty)}]$ has kernel defined from equation (23) in Lemma 1, considering $\omega_i = \omega_j = 0$.

Proof. See Section A.1 of Appendices.

3 Second and fourth order bias asymptotics under LRD

New results on the bias asymptotics of the integrated second and fourth order empirical cumulant spectral density operators of X under H_1 are obtained in this section. These results will be applied in the next section for deriving Theorem 2 and Corollary 2, providing the consistency of the integrated weighted periodogram operator under the LRD setting assumed in H_1 . In all the subsequent results in the next sections, we assume $B_T \rightarrow 0$ and $B_T T \rightarrow \infty$ as $T \rightarrow \infty$.

The rate of convergence to zero of the bias of the integrated periodogram operator in the space $\mathcal{S}(L^2(\mathbb{M}_d, d\nu, \mathbb{C}))$ is obtained under LRD in the next lemma. The proof of this result exploits (16), in a similar way to Theorem 1 in [32], and the tools available in our particular manifold setting (see Section B.1 of the Appendices). The following well-known identity will be applied:

$$\mathcal{F}_\omega^{(T)} = E[\mathcal{P}_\omega^{(T)}] = [F_T * \mathcal{F}_\bullet](\omega) = \int_{-\pi}^{\pi} F_T(\omega - \xi) \mathcal{F}_\xi d\xi, \quad T \geq 2, \quad (25)$$

for $\omega \in [-\pi, \pi] \setminus \{0\}$, where $F_T(\omega)$ denotes the Féjer kernel in equation (5) of Section 1.1.

Lemma 2 Under H_1 , as $T \rightarrow \infty$,

$$\int_{-\pi}^{\pi} \mathcal{F}_\omega^{(T)} d\omega = \int_{-\pi}^{\pi} E_{H_1}[\mathcal{P}_\omega^{(T)}] d\omega \underset{\mathcal{S}(L^2(\mathbb{M}_d, d\nu, \mathbb{C}))}{=} \int_{-\pi}^{\pi} \mathcal{F}_\omega d\omega + \mathcal{O}(T^{-1}), \quad (26)$$

where E_{H_1} denotes expectation under the alternative H_1 .

Proof. See Section B.1 of the Appendices.

The following corollary is obtained from Lemma 2, and provides the rate of convergence to zero of the bias of the integrated weighted periodogram operator, in the norm of $\mathcal{S}(L^2(\mathbb{M}_d, d\nu, \mathbb{C}))$, under H_1 .

Corollary 1 Under H_1 , as $T \rightarrow \infty$,

$$\int_{-\pi}^{\pi} E_{H_1}[\widehat{\mathcal{F}}_{\omega}^{(T)}] d\omega \underset{\mathcal{S}(L^2(\mathbb{M}_d, d\nu, \mathbb{C}))}{=} \int_{-\pi}^{\pi} \int_{\mathbb{R}} W(\xi) \mathcal{F}_{\omega - \xi B_T} d\xi d\omega + \mathcal{O}(B_T^{-1} T^{-1}) + \mathcal{O}(T^{-1}). \quad (27)$$

Proof. See Section B.2 of the Appendices.

The rate of convergence to zero, in the space $\mathcal{S}(L^2(\mathbb{M}_d^2, \otimes_{i=1}^2 \nu(dx_i), \mathbb{C})) \equiv L^2(\mathbb{M}_d^4, \otimes_{i=1}^4 \nu(dx_i), \mathbb{C})$, of the bias of the integrated fourth-order empirical cumulant spectral density operators of X under LRD is obtained in Lemma 3 below. The following assumption is required:

Assumption I. For every $t_1, t_2, t_3 \in \mathbb{Z}$, $\text{cum}(X_{t_1}, X_{t_2}, X_{t_3}, X_0)$ defines an isotropic kernel in $L^2(\mathbb{M}_d^4, \otimes_{i=1}^4 d\nu(dx_i), \mathbb{R})$, and the following convergence holds:

$$\sum_{t_1, t_2, t_3 \in \mathbb{Z}} \|\text{cum}(X_{t_1}, X_{t_2}, X_{t_3}, X_0)\|_{L^2(\mathbb{M}_d^4, \otimes_{i=1}^4 d\nu(x_i), \mathbb{R})}^2 < \infty, \quad (28)$$

where

$$\begin{aligned} & \|\text{cum}(X_{t_1}, X_{t_2}, X_{t_3}, X_0)\|_{L^2(\mathbb{M}_d^4, \otimes_{i=1}^4 d\nu(dx_i), \mathbb{R})}^2 \\ &= \int_{\mathbb{M}_d^4} |\text{cum}(X_{t_1}(x), X_{t_2}(y), X_{t_3}(z), X_0(v))|^2 d\nu(x) d\nu(y) d\nu(z) d\nu(v). \end{aligned}$$

Lemma 3 Under H_1 and Assumption I, uniformly in $\omega_4 \in [-\pi, \pi]$,

$$\begin{aligned} & \int_{[-\pi, \pi]^3} T \text{cum}\left(\widetilde{X}_{\omega_1}^{(T)}(\tau_1), \widetilde{X}_{\omega_2}^{(T)}(\tau_2), \widetilde{X}_{\omega_3}^{(T)}(\tau_3), \widetilde{X}_{\omega_4}^{(T)}(\tau_4)\right) d\omega_1 d\omega_2 d\omega_3 \\ & \underset{\mathcal{S}(L^2(\mathbb{M}_d^2, \otimes_{i=1}^2 \nu(dx_i), \mathbb{C}))}{=} 2\pi \int_{[-\pi, \pi]^3} \mathcal{F}_{\omega_1, \omega_2, \omega_3}(\tau_1, \tau_2, \tau_3, \tau_4) d\omega_1 d\omega_2 d\omega_3 + \mathcal{O}(T^{-1}), \end{aligned} \quad (29)$$

where, for $\omega_i \in [-\pi, \pi]$, $i = 1, 2, 3$,

$$\mathcal{F}_{\omega_1, \omega_2, \omega_3} \underset{\mathcal{S}(L^2(\mathbb{M}_d^2, \otimes_{i=1}^2 \nu(dx_i), \mathbb{C}))}{=} \frac{1}{(2\pi)^3} \sum_{t_1, t_2, t_3 = -\infty}^{\infty} \exp\left(\sum_{j=1}^3 \omega_j t_j\right) \text{cum}(X_{t_1}, X_{t_2}, X_{t_3}, X_0) \quad (30)$$

denotes the cumulant spectral density operator of order 4 of X , and, as before,
 $\overset{=}{S(L^2(\mathbb{M}_d^2, \otimes_{i=1}^2 \nu(dx_i), \mathbb{C}))}$ means the identity in the space $\mathcal{S}(L^2(\mathbb{M}_d^2, \otimes_{i=1}^2 \nu(dx_i), \mathbb{C})) \equiv L^2(\mathbb{M}_d^4, \otimes_{i=1}^4 d\nu(x_i), \mathbb{C})$.

Proof. See Section B.3 of the Appendices.

4 A test for LRD in \mathbb{M}_d -supported functional time series

Consistency of the test based on \mathcal{S}_{B_T} is derived in this section. Specifically, Theorem 3 provides the almost surely divergence in the norm of the space $\mathcal{S}(L^2(\mathbb{M}_d, d\nu, \mathbb{C}))$ of \mathcal{S}_{B_T} under H_1 . The proof of this result follows from Proposition 1, showing the divergence in the norm of the space $\mathcal{S}(L^2(\mathbb{M}_d, d\nu, \mathbb{C}))$ of the centering operator of \mathcal{S}_{B_T} , and from Theorem 2 and Corollary 2, establishing the consistency of the integrated weighted periodogram operator under H_1 . The implementation of the testing procedure in practice is also discussed.

Proposition 1 Under H_1 , as $T \rightarrow \infty$,

$$\left\| \int_{[-\sqrt{B_T}/2, \sqrt{B_T}/2]} E_{H_1}[\widehat{\mathcal{F}}_\omega^{(T)}] \frac{d\omega}{\sqrt{B_T}} \right\|_{\mathcal{S}(L^2(\mathbb{M}_d, d\nu, \mathbb{C}))} \geq g(T) = \mathcal{O}(B_T^{-l_\alpha - 1/2}). \quad (31)$$

Proof. See Section C.1 of the Appendices.

Theorem 2 Under H_1 , Assumption I, and

$$\int_{[-\pi, \pi]} \|\mathcal{M}_\omega\|_{L^1(L^2(\mathbb{M}_d, d\nu, \mathbb{C}))}^2 |\omega|^{-2L_\alpha} d\omega < \infty, \quad (32)$$

as $T \rightarrow \infty$,

$$\int_{-\pi}^{\pi} E_{H_1} \left\| \widehat{\mathcal{F}}_\omega^{(T)} - E_{H_1}[\widehat{\mathcal{F}}_\omega^{(T)}] \right\|_{\mathcal{S}(L^2(\mathbb{M}_d, d\nu, \mathbb{C}))}^2 d\omega \leq h(T) = \mathcal{O}(B_T^{-1} T^{-1}), \quad (33)$$

where, as before, $\|\cdot\|_{L^1(L^2(\mathbb{M}_d, d\nu, \mathbb{C}))}$ denotes the norm in the space $L^1(L^2(\mathbb{M}_d, d\nu, \mathbb{C}))$ of nuclear operators on $L^2(\mathbb{M}_d, d\nu, \mathbb{C})$.

Remark 1 Note that condition (32) is satisfied, for instance, when the family $\{\mathcal{M}_\omega, \omega \in [-\pi, \pi]\}$ lies in a ball of radius $R > 0$ of the space $L^1(L^2(\mathbb{M}_d, d\nu, \mathbb{C}))$.

Proof. See Section C.2 of the Appendices.

Theorem 2 implies the weak consistency of the integrated weighted periodogram operator under H_1 in the norm of the space $\mathcal{S}(L^2(\mathbb{M}_d, d\nu, \mathbb{C}))$.

Corollary 2 Under the conditions of Theorem 2, as $T \rightarrow \infty$,

$$\left\| \int_{-\pi}^{\pi} E_{H_1} \left[\widehat{\mathcal{F}}_\omega^{(T)} - \int_{-\pi}^{\pi} W(\xi) \mathcal{F}_{\omega - B_T \xi} d\xi \right] d\omega \right\|_{\mathcal{S}(L^2(\mathbb{M}_d, d\nu, \mathbb{C}))} \leq \widetilde{g}(T) = \mathcal{O}(T^{-1/2} B_T^{-1/2}).$$

Proof. See Section C.3 of the Appendices.

Under the conditions assumed in the following result, \mathcal{S}_{B_T} in (21) allows to testing (19)–(20) in a consistent way.

Theorem 3 Under H_1 , assume that $l_\alpha > 1/4$, and that the bandwidth parameter $B_T = T^{-\beta}$ for $\beta \in (0, 1)$. If conditions of Theorem 2 hold, then, as $T \rightarrow \infty$,

$$\|\mathcal{S}_{B_T}\|_{\mathcal{S}(L^2(\mathbb{M}_d, d\nu, \mathbb{C}))} \rightarrow a.s. \infty,$$

where $\rightarrow a.s. \infty$ denotes almost surely divergence.

Proof. See Section C.4 of the Appendices.

4.1 Practical implementation

The practical implementation of the proposed testing approach is now briefly discussed, contemplating Gaussian random projection methodology (see Theorem 4.1 in [5]). In our context, this methodology can be implemented from Lemma 4 below. This lemma provides the Karhunen–Loève expansion of the $\mathcal{S}(L^2(\mathbb{M}_d, d\nu, \mathbb{C}))$ -valued zero-mean Gaussian random elements in the spectral family characterized in equation (23) of Lemma 1. The involved random Fourier coefficients are defined as follows:

$$Y_{n,j,h,l}(\omega) = \frac{(\sqrt{2\pi} \|W\|_{L^2(\mathbb{R})})^{-1}}{\sqrt{f_n(\omega) f_h(\omega)}} \int_{\mathbb{M}_d^2} \widehat{f}_\omega(\tau, \sigma) \overline{S_{n,j}^d(\tau)} S_{h,l}^d(\sigma) d\nu(\sigma) d\nu(\tau),$$

$$j = 1, \dots, \Gamma(n, d), \quad l = 1, \dots, \Gamma(h, d), \quad n, h \in \mathbb{N}_0, \quad \omega \in (-\pi, \pi) \setminus \{0\},$$
(34)

where integration is understood in the mean-square sense.

Lemma 4 Let \widehat{f}_ω be the kernel of a zero-mean Gaussian random operator, in the space $\mathcal{S}(L^2(\mathbb{M}_d, d\nu, \mathbb{C}))$, satisfying equation (23) of Lemma 1. Then, the following series expansion holds in the mean-square sense: For every $(\tau, \sigma) \in \mathbb{M}_d^2$,

$$\begin{aligned} \frac{1}{\sqrt{2\pi}\|W\|_{L^2(\mathbb{R})}} \widehat{f}_\omega(\tau, \sigma) &= \mathcal{L}_{\mathcal{S}(L^2(\mathbb{M}_d, d\nu; \mathbb{C}))}^2(\Omega, \mathcal{A}, \mathcal{P}) \sum_{n, h \in \mathbb{N}_0} \sum_{j=1}^{\Gamma(n, d)} \sum_{l=1}^{\Gamma(h, d)} \sqrt{f_n(\omega) f_h(\omega)} \\ &\quad \times Y_{n, j, h, l}(\omega) S_{n, j}^d(\tau) \overline{S_{h, l}^d(\sigma)}, \quad \omega \in (-\pi, \pi) \setminus \{0\}, \end{aligned} \quad (35)$$

where, as before, $\mathcal{L}_{\mathcal{S}(L^2(\mathbb{M}_d, d\nu; \mathbb{C}))}^2(\Omega, \mathcal{A}, \mathcal{P})$ denotes the space of zero-mean second-order $\mathcal{S}(L^2(\mathbb{M}_d, d\nu; \mathbb{C}))$ -valued random variables with the norm $\sqrt{E\|\cdot\|_{\mathcal{S}(L^2(\mathbb{M}_d, d\nu; \mathbb{C}))}^2}$. The random Fourier coefficients

$$\{Y_{n, j, h, l}(\omega), \quad j = 1, \dots, \Gamma(n, d), \quad l = 1, \dots, \Gamma(h, d), \quad n, h \in \mathbb{N}_0\},$$

for $\omega \in (-\pi, \pi) \setminus \{0\}$, have been introduced in equation (34). They are independent and identically distributed standard Gaussian complex-valued random variables.

Proof. See Section C.5 of the Appendices.

Theorem 3 motivates the methodology to be adopted in practice. Specifically, as illustrated in the simulation study undertaken in the next section, a consistent test for LRD is obtained by rejecting H_0 , when, for every $j = 1, \dots, \Gamma(n, d)$, $l = 1, \dots, \Gamma(h, d)$, $n, h \in \mathbb{N}_0$,

$$\frac{\left| [\mathcal{S}_{B_T} - E[\mathcal{S}_{B_T}]](\overline{S_{h, l}^d})(S_{n, j}^d) \right|}{\sqrt{\text{Var}\left(\mathcal{S}_{B_T}(\overline{S_{h, l}^d})(S_{n, j}^d)\right)}} \quad (36)$$

is larger than an upper tail standard normal critical value. Note that for T

sufficiently large,

$$\begin{aligned}
[\mathcal{S}_{B_T} - E[\mathcal{S}_{B_T}]](\overline{S_{h,l}^d})(S_{n,j}^d) &= \int_{\mathbb{M}_d^2} [\mathcal{S}_{B_T} - E[\mathcal{S}_{B_T}]](\tau, \sigma) \overline{S_{n,j}^d}(\tau) S_{h,l}^d(\sigma) d\nu(\sigma) d\nu(\tau) \\
\text{Var} \left(\mathcal{S}_{B_T}(\overline{S_{h,l}^d})(S_{n,j}^d) \right) &= \text{Var} \left(\int_{\mathbb{M}_d^2} \mathcal{S}_{B_T}(\tau, \sigma) \overline{S_{n,j}^d}(\tau) S_{h,l}^d(\sigma) d\nu(\sigma) d\nu(\tau) \right) \\
&= 2\pi \int_{[-\sqrt{B_T}/2, \sqrt{B_T}/2]^2 \times [-\pi, \pi]} W\left(\frac{\omega - \alpha}{B_T}\right) \left[W\left(\frac{\xi - \alpha}{B_T}\right) + W\left(\frac{\xi + \alpha}{B_T}\right) \right. \\
&\quad \times \left\langle S_{n,j}^d, \overline{S_{h,l}^d} \right\rangle_{L^2(\mathbb{M}_d, d\nu, \mathbb{C})} \left\langle \overline{S_{n,j}^d}, S_{h,l}^d \right\rangle_{L^2(\mathbb{M}_d, d\nu, \mathbb{C})} \left. f_n(\alpha) f_h(\alpha) \frac{d\alpha d\omega d\xi}{B_T^2} \right. \\
&\quad \left. + \mathcal{O}(B_T^{-2} T^{-2}) + \mathcal{O}(T^{-1}) \right], \quad j = 1, \dots, \Gamma(n, d), \quad l = 1, \dots, \Gamma(h, d), \quad n, h \in \mathbb{N}_0.
\end{aligned} \tag{37}$$

The dimensionality problem associated with this testing procedure can be substantially alleviated if we restrict our attention to the case where all moments of \mathcal{S}_{B_T} are finite and satisfy the Carleman condition. In that case, one can apply Theorem 4.1 in [5], allowing the testing procedure to be implemented, conditionally to the functional value \mathbf{k} generated from an $\mathcal{S}(L^2(\mathbb{M}_d, d\nu; \mathbb{C}))$ -valued Gaussian random variable, with probability measure μ on $\mathcal{S}(L^2(\mathbb{M}_d, d\nu; \mathbb{C}))$. Specifically, H_0 is tested, in terms of $H_0^{\mathbf{k}}$, from the random projected statistics

$$\mathcal{T}_{B_T}^{\mathbf{k}} = \frac{\left| \langle \mathcal{S}_{B_T} - E[\mathcal{S}_{B_T}], \mathbf{k} \rangle_{\mathcal{S}(L^2(\mathbb{M}_d, d\nu; \mathbb{C}))} \right|}{\sqrt{\text{Var} \left(\langle \mathcal{S}_{B_T} - E[\mathcal{S}_{B_T}], \mathbf{k} \rangle_{\mathcal{S}(L^2(\mathbb{M}_d, d\nu; \mathbb{C}))} \right)}}. \tag{38}$$

According to Theorem 4.1 in [5] (see also [6]), if H_0 holds, then $H_0^{\mathbf{k}}$ also holds, and if H_0 fails then $H_0^{\mathbf{k}}$ also fails μ -a.s. Thus, with probability one, we will generate a realization of random direction \mathbf{k} in $\mathcal{S}(L^2(\mathbb{M}_d, d\nu; \mathbb{C}))$ for which $H_0^{\mathbf{k}}$ fails. As before, $H_0^{\mathbf{k}}$ will be rejected if the observed value of $\mathcal{T}_{B_T}^{\mathbf{k}}$ is larger than an upper tail standard normal critical value.

For different values of indexes $j = 1, \dots, \Gamma(n, d)$, $l = 1, \dots, \Gamma(h, d)$, $n, h \in \mathbb{N}_0$, different Gaussian random directions in $\mathcal{S}(L^2(\mathbb{M}_d, d\nu; \mathbb{C}))$ can be defined from

$$\mathbf{k}_{n,j,h,l}(\tau, \sigma) = Y_{n,j,h,l}[S_{n,j}^d \otimes \overline{S_{h,l}^d}(\tau, \sigma)], \quad (\tau, \sigma) \in \mathbb{M}_d^2, \tag{39}$$

where $Y_{n,j,h,l}$ denotes a zero-mean Gaussian random variable with variance $\lambda_{n,h}$ (see also [21] on Gaussian random spherical harmonics). The Gaussian random directions involved in the eigenspaces, where stronger persistency in time is observed, play a key role in this testing procedure. Furthermore, if we assume that $\sum_{n \in \mathbb{N}_0} \sum_{h \in \mathbb{N}_0} \Gamma(n, d) \Gamma(h, d) \lambda_{n,h} < \infty$, Lemma 4 provides a way to

generate \mathbf{k} from the Karhunen–Loève expansion. That is, one can consider \mathbf{k} to be a zero–mean Gaussian random element in $\mathcal{S}(L^2(\mathbb{M}_d, d\nu; \mathbb{C}))$ satisfying (35), with covariance operator $C_{\mathbf{k}}$ having covariance kernel, given by, for every $(\tau_1, \sigma_1), (\tau_2, \sigma_2) \in \mathbb{M}_d^2$,

$$\begin{aligned} C_{\mathbf{k}}(\tau_1, \sigma_1, \tau_2, \sigma_2) &= E[\mathbf{k}(\tau_1, \sigma_1)\mathbf{k}(\tau_2, \sigma_2)] \\ &= \sum_{n \in \mathbb{N}_0} \sum_{j=1}^{\Gamma(n,d)} \sum_{h \in \mathbb{N}_0} \sum_{l=1}^{\Gamma(h,d)} \lambda_{n,h} S_{n,j}^d(\tau_1) \overline{S_{h,l}^d(\sigma_1)} S_{n,j}^d(\tau_2) S_{h,l}^d(\sigma_2). \end{aligned} \quad (40)$$

The large functional sample size properties of \mathcal{S}_{B_T} in (21) are numerically illustrated in the next section by simulations, paying special attention to the illustration of Theorems 1 and 3. Robust empirical sizes, and good empirical power properties are also observed for finite functional sample sizes.

5 Simulation study

Our simulations will be set on $\mathbb{M}_d = \mathbb{S}_d \subset \mathbb{R}^{d+1}$. An alternative generation algorithm to the ones considered in [22] and [23] is implemented reducing computational burden allowing for the consideration of large functional sample sizes. Theorem 1 is illustrated in the context of SPHARMA(p,q) processes, and the illustration of Theorem 3 is carried out in the context of multifractionally integrated SPHARMA(p,q) processes. These numerical results are respectively reported in Sections 5.1 and 5.2 for $\beta = 1/4$, i.e., $B_T = T^{-1/4}$ (see also Section 6 for a wider analysis for different β values). When $L_\alpha > 1/2$, Section 5.3 opens new research lines beyond condition (16), providing empirical evidence of a faster a.s. divergence rate of \mathcal{S}_{B_T} in the norm of the space $\mathcal{S}(L^2(\mathbb{M}_d, d\nu; \mathbb{C}))$. Finally, Section 5.4 shows empirical size and power properties of the testing procedure.

5.1 Asymptotic Gaussian distribution of \mathcal{S}_{B_T} under H_0

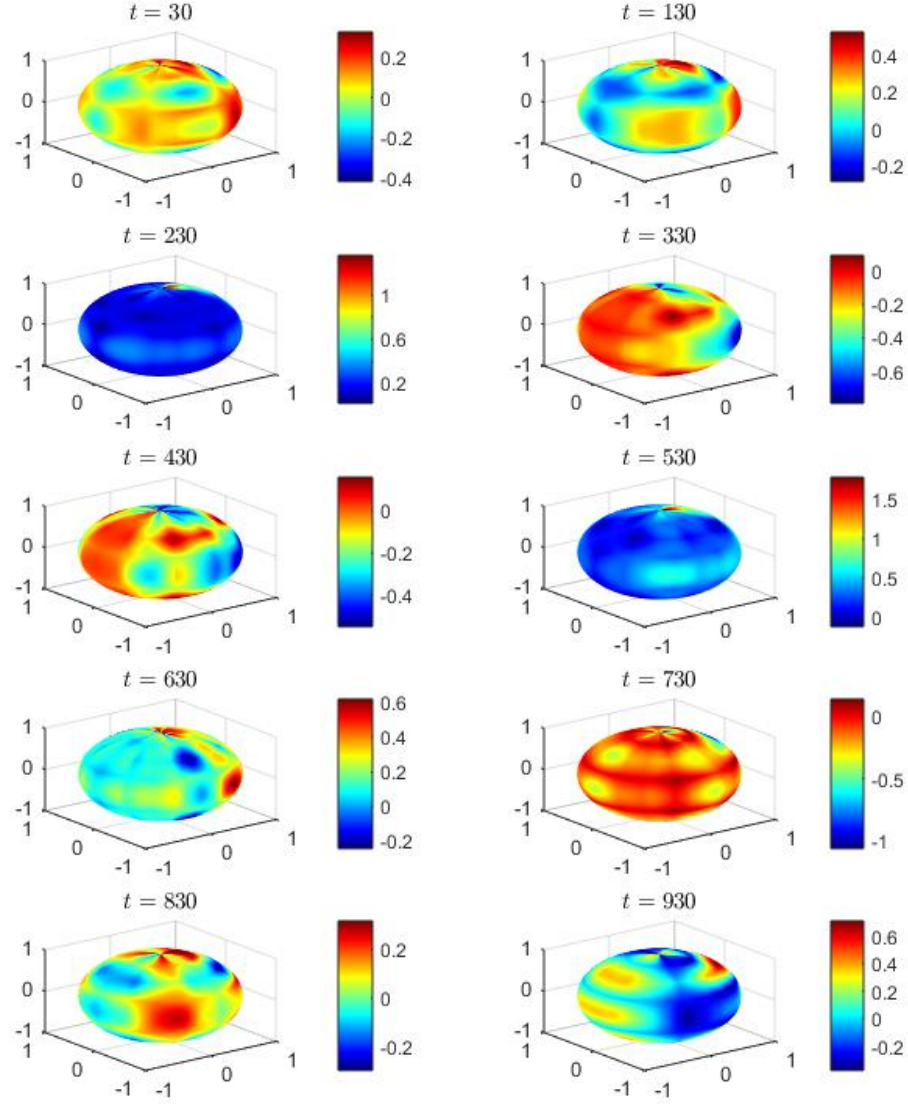


Figure 1: One realization at times $t = 30, 130, 230, 330, 430, 530, 630, 730, 830, 930$ of SPHARMA(1,1) process $\left(\lambda_n(\varphi_1) = 0.7 \left(\frac{n+1}{n}\right)^{-3/2}$, and $\lambda_n(\psi_1) = (0.4) \left(\frac{n+1}{n}\right)^{-5/1.95}$, $n = 1, 2, 3, 4, 5, 6, 7, 8$), projected into the direct sum $\bigoplus_{n=1}^8 \mathcal{H}_n$ of eigenspaces \mathcal{H}_n , $n = 1, \dots, 8$, of Δ_2

Let us consider that the elements of the family of spectral density operators of X have frequency varying eigenvalues, with respect to the system of eigenfunctions of the Laplace–Beltrami operator, obeying the following equation under H_0 (see [32]):

$$f_n(\omega) = \frac{\lambda_n(\mathcal{R}_0^\eta)}{2\pi} \left| \frac{\Psi_{q,n}(\exp(-i\omega))}{\Phi_{p,n}(\exp(-i\omega))} \right|^2, \quad n \in \mathbb{N}_0, \quad \omega \in [-\pi, \pi], \quad (41)$$

where $\{\lambda_n(\mathcal{R}_0^\eta), n \in \mathbb{N}_0\}$ is the system of eigenvalues of the autocovariance operator \mathcal{R}_0^η of the innovation process $\eta = \{\eta_t, t \in \mathbb{Z}\}$, with respect to the system of eigenfunctions of the Laplace–Beltrami operator. Process η is assumed to be strong–white noise in $L^2(\mathbb{S}_d, d\nu, \mathbb{R})$. That is, η is assumed to be a sequence of independent and identically distributed $L^2(\mathbb{S}_d, d\nu, \mathbb{R})$ –valued random variables such that $E[\eta_t] = 0$, and $E[\eta_t \otimes \eta_s] = \delta_{t,s} \mathcal{R}_0^\eta$, with $\mathcal{R}_0^\eta \in L^1(L^2(\mathbb{S}_d, d\nu, \mathbb{R}))$, and $\delta_{t,s} = 0$, for $t \neq s$, and $\delta_{t,s} = 1$, for $t = s$. For $n \in \mathbb{N}_0$, $\Phi_{p,n}(z) = 1 - \sum_{j=1}^p \lambda_n(\varphi_j) z^j$ and $\Psi_{q,n}(z) = \sum_{j=1}^q \lambda_n(\psi_j) z^j$, with $\{\lambda_n(\varphi_j), n \in \mathbb{N}_0\}$ and $\{\lambda_n(\psi_l), n \in \mathbb{N}_0\}$ denoting the sequences of eigenvalues, with respect to the system of eigenfunctions of the Laplace–Beltrami operator, of the self–adjoint invariant integral operators φ_j and ψ_l , for $j = 1, \dots, p$, and $l = 1, \dots, q$, respectively. These operators satisfy the following equations:

$$\Phi_p(B) = 1 - \sum_{j=1}^p \varphi_j B^j, \quad \Psi_q(B) = \sum_{j=1}^q \psi_j B^j,$$

where B is a difference operator such that

$$E\|B^j X_t - X_{t-j}\|_{L^2(\mathbb{S}_d, d\nu, \mathbb{R})}^2 = 0, \quad \forall t, j \in \mathbb{Z}. \quad (42)$$

Here, Φ_p and Ψ_q are the so–called autoregressive and moving average operators, respectively. Also, for each $n \in \mathbb{N}_0$, $\Phi_{p,n}(z) = 1 - \sum_{j=1}^p \lambda_n(\varphi_j) z^j$ and $\Psi_{q,n}(z) = \sum_{j=1}^q \lambda_n(\psi_j) z^j$ have not common roots, and their roots are outside of the unit circle (see also Corollary 6.17 in [1]). Thus, X satisfies an SPHARMA(p,q) equation (see also [2]; [3]).

In the simulations we have generated an SPHARMA(1,1) process, i.e., $p = q = 1$, with $H = L^2(\mathbb{S}_2, d\nu, \mathbb{R})$, and $\lambda_n(\varphi_1) = 0.7 \left(\frac{n+1}{n}\right)^{-3/2}$ and $\lambda_n(\psi_1) = (0.4) \left(\frac{n+1}{n}\right)^{-5/1.95}$, $n \in \mathbb{N}_0$. Figure 1 displays one realization of the generated SPHARMA(1,1) process projected into $\bigoplus_{n=1}^8 \mathcal{H}_n$, at times $t = 30, 130, 230, 330, 430, 530, 630, 730, 830, 930$.

The empirical distribution of the centered and standardized projections of \mathcal{S}_{B_T} into $\mathcal{H}_n \otimes \mathcal{H}_n$, for each $n = 1, \dots, 8$, are displayed for functional sample

size $T = 1000$ and $R = 3000$ repetitions in Figure 2, for functional sample size $T = 2000$ and $R = 3000$ repetitions in Figure 3, and for functional sample size $T = 3000$ and $R = 3000$ repetitions in Figure 4. These empirical distributions approximate the support and shape of a standard Gaussian probability density. The empirical standardization displays a decreasing pattern over the spherical scale n , meaning that the respective limit one-dimensional Gaussian probability measures of these projections have decreasing support. According to Theorem 1.2.1 in [7], this property is satisfied by the infinite product Gaussian measure on $(\mathbb{R}^\infty, \mathcal{B}(\mathbb{R}^\infty))$, whose restriction to $L^2(\mathbb{S}_d, d\nu, \mathbb{C})$ is identified in ℓ^2 -sense with the probability measure of the limit Gaussian random element in Theorem 1.

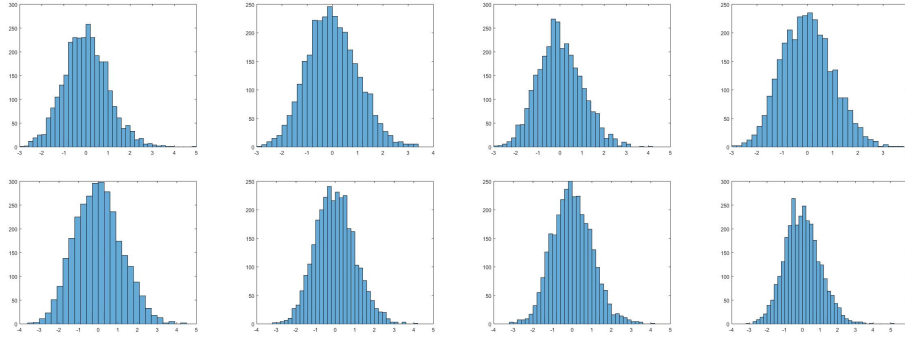


Figure 2: Empirical projections of the probability measure of standardized \mathcal{S}_{B_T} , $B_T = T^{-1/4}$, under H_0 , into the eigenspaces $\mathcal{H}_n \otimes \mathcal{H}_n$, for $n = 1, 2, 3, 4, 5, 6, 7, 8$, respectively displayed from the left to the right, and from the top to the bottom, for functional samples size $T = 1000$ and $R = 3000$ repetitions

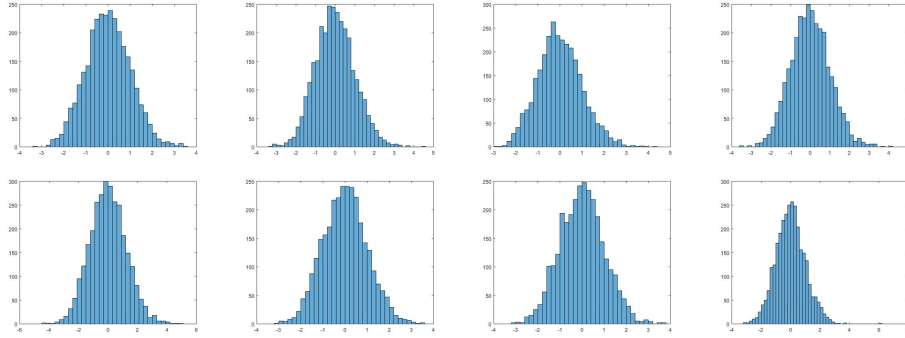


Figure 3: Empirical projections of the probability measure of standardized \mathcal{S}_{B_T} , $B_T = T^{-1/4}$, under H_0 , into the eigenspaces $\mathcal{H}_n \otimes \mathcal{H}_n$, for $n = 1, 2, 3, 4, 5, 6, 7, 8$, respectively displayed from the left to the right, and from the top to the bottom, for functional samples size $T = 2000$ and $R = 3000$ repetitions

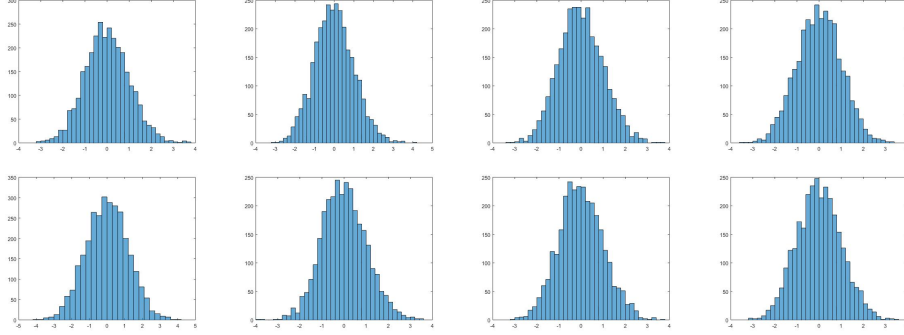


Figure 4: Empirical projections of the probability measure of standardized \mathcal{S}_{B_T} , $B_T = T^{-1/4}$, under H_0 , into the eigenspaces $\mathcal{H}_n \otimes \mathcal{H}_n$, for $n = 1, 2, 3, 4, 5, 6, 7, 8$, respectively displayed from the left to the right, and from the top to the bottom, for functional samples size $T = 3000$ and $R = 3000$ repetitions

5.2 Consistency of the test

Under H_1 , for each $\omega \in [-\pi, \pi]$, the eigenvalues $\{f_n(\omega), n \in \mathbb{N}_0\}$ satisfy (see equations (17), (18) and (20))

$$f_n(\omega) = \frac{\lambda_n(\mathcal{R}_0^\eta)}{2\pi} \left| \frac{\Psi_{q,n}(\exp(-i\omega))}{\Phi_{p,n}(\exp(-i\omega))} \right|^2 |1 - \exp(-i\omega)|^{-\alpha(n)}, \quad n \in \mathbb{N}_0. \quad (43)$$

Again, we consider the projection of X into $\bigoplus_{n=1}^8 \mathcal{H}_n$. Three multifractional integration operators, applied to SPHARMA(1,1) process generated in Section 5.1, are considered in Sections 5.2.1–5.2.3. In Example 1, $\alpha(n)$ is decreasing over n , in Example 2 $\alpha(n)$ is increasing over n , and non-monotone in Example 3. Note that, under the generated Gaussian scenario, condition (16) implies that Assumption I holds. Furthermore, condition (32) also holds since φ_1 lies in the unit ball of the space $\mathcal{L}(L^2(\mathbb{S}_2, d\nu, \mathbb{C}))$, and ψ_1 belongs to the trace class. The figures of Sections 5.2.1–5.2.3 are respectively displayed in Sections D.1.1–D.1.3 of the Appendices.

5.2.1 Example 1

Theorem 3 is now illustrated in the case where the largest dependence range is displayed by the process projected into the eigenspace \mathcal{H}_1 . Figure 1 in Section D.1.1 of the Appendices displays a sample realization of multifractionally integrated SPHARMA (1,1) process X projected into $\bigoplus_{i=1}^8 \mathcal{H}_i$. In this example, $L_\alpha = 0.4733$, $l_\alpha = 0.2678$, and $\alpha(n) = l_\alpha = 0.2678$, $n \geq 9$ (see plot at the left-hand side of Figure 2 in Section D.1.1 of the Appendices). The a.s. divergence of \mathcal{S}_{B_T} , for $B_T = T^{-1/4}$, in the Hilbert–Schmidt operator norm (see Table 1)

is also reflected in the observed increasing sample values of each one of its projections into $\mathcal{H}_n \otimes \mathcal{H}_n$, $n = 1, \dots, 8$, for the increasing functional samples sizes $T = 1000, 10000, 30000$ (see the three plots at the right-hand side of Figure 2 in Section D.1.1 of the Appendices).

5.2.2 Example 2

The dominant subspace in this example, where the projected process displays the largest dependence range, is eigenspace \mathcal{H}_8 . One sample realization of the generated multifractionally integrated SPHARMA (1,1) process, projected into $\bigoplus_{n=1}^8 \mathcal{H}_n$, is displayed in Figure 3 in Section D.1.2 of the Appendices. The LRD operator eigenvalues $\alpha(n)$, $n = 1, 2, 3, 4, 5, 6, 7, 8$, are given in the plot at the left-hand side of Figure 4 in Section D.1.2 of the Appendices, where $L_\alpha = 0.3327$, $l_\alpha = 0.2550$, and $\alpha(n) = l_\alpha = 0.2550$, $n \geq 9$. The a.s. divergence of our test statistics operator in the Hilbert–Schmidt operator norm (see also Table 1) is illustrated in the three plots at the right-hand side of such Figure 4, in terms of the sample values of each projection of \mathcal{S}_{B_T} , $B_T = T^{-1/4}$, into $\mathcal{H}_n \otimes \mathcal{H}_n$, $n = 1, \dots, 8$, for increasing functional samples sizes $T = 1000, 10000, 30000$.

5.2.3 Example 3

In this third example, the dominant subspace is eigenspace \mathcal{H}_5 of the Laplace–Beltrami operator Δ_2 . One sample realization of the generated multifractionally integrated SPHARMA (1,1) process, projected into $\bigoplus_{n=1}^8 \mathcal{H}_n$, is displayed in Figure 5 in Section D.1.3 of the Appendices. The eigenvalues $\alpha(n)$, $n = 1, 2, 3, 4, 5, 6, 7, 8$, of LRD operator \mathcal{A} are showed in the plot at the left-hand side of Figure 6 in Section D.1.3 of the Appendices, with $L_\alpha = 0.4000$, and $l_\alpha = 0.2753 = \alpha(n)$, $n \geq 9$. The sample values of the projections of \mathcal{S}_{B_T} , $B_T = T^{-1/4}$, into $\mathcal{H}_n \otimes \mathcal{H}_n$, $n = 1, \dots, 8$, for functional samples sizes $T = 1000, 10000, 30000$, can be found in the three plots at the right-hand side of Figure 6 (see also Table 1).

5.2.4 Almost surely divergence of \mathcal{S}_{B_T} in $\mathcal{S}(L^2(\mathbb{M}_d, d\nu, \mathbb{C}))$ norm under H_1

The observed Hilbert–Schmidt operator norm of \mathcal{S}_{B_T} , for $B_T = T^{-1/4}$, projected into $\bigoplus_{n=1}^8 \mathcal{H}_n \otimes \mathcal{H}_n$, is displayed in Table 1, for the three numerical examples generated, and for the functional sample sizes $T = 1000, 5000, 10000, 30000, 50000, 100000$. One can observe in Table 1 the increasing sample values of the Hilbert–Schmidt operator norm of the projected \mathcal{S}_{B_T} as T increases, in all the examples under $l_\alpha > 1/4$, with $B_T = T^{-\beta}$, $\beta = 1/4$, satisfying $TB_T \rightarrow \infty$, $T \rightarrow \infty$.

Table 1: $\|\mathcal{S}_{B_T}\|$, $\beta = 1/4$

T	Example 1	Example 2	Example 3
1000	2.3036e+05	2.2595e+05	1.9934e+05
5000	1.0612e+07	1.0223e+07	9.0697e+06
10000	5.5172e+07	5.3770e+07	4.7303e+07
30000	7.5695e+08	7.3377e+08	6.4742e+08
50000	2.5516e+09	2.4764e+09	2.1844e+09
100000	1.3256e+10	1.2892e+10	1.2906e+10

Spherical sample patterns and scales induced by the multifractional integration operator (see Figures 1, 3 and 5 in Sections D.1.1–D.1.3 of the Appendices, respectively) have no significant effect (see Table 1), when the condition $l_\alpha > 1/4$ is satisfied under the bandwidth parameter modelling $B_T = T^{-\beta}$, $\beta \in (0, 1)$. This fact is also reflected in Figures 2, 4 and 6 in Sections D.1.1–D.1.3 of the Appendices, respectively, where decreasing patterns, and almost the same divergence rates are displayed by the sample values of \mathcal{S}_{B_T} projected into $\mathcal{H}_n \otimes \mathcal{H}_n$, for $n = 1, 2, 3, 4, 5, 6, 7, 8$, in all the examples. However, the scenario under which $\alpha(n)$ crosses the threshold $1/2$ at some spherical scale n requires a separated analysis, as briefly discussed in Example 4 in the next section (see Figure 8 in Section D.1.4 of the Appendices).

5.3 Example 4

Our numerical analysis is extended here beyond the restriction $L_\alpha < 1/2$. Specifically, this section shows some preliminary numerical results regarding the effect of higher levels of singularity at zero frequency when $L_\alpha > 1/2$, i.e., $\|\mathcal{A}\|_{\mathcal{L}(L^2(\mathbb{S}_2, d\nu; \mathbb{C}))} > 1/2$, corresponding to a stronger persistency in time of the projected process into the dominant subspace (see Figure 7 in Section D.1.4 of the Appendices). Under this scenario, conditions (16), and (32) in Theorem 2, are not satisfied. Indeed, we are out of the scenario where the summability in time of the square of the Hilbert–Schmidt operator norms of the elements of the covariance operator family holds. Then, new technical tools are required to address the asymptotic analysis in the spectral domain of this family of manifold supported functional time series displaying stronger levels of persistency in time.

Let us again consider \mathcal{S}_{B_T} , for $B_T = T^{-1/4}$, projected into $\bigoplus_{n=1}^8 \mathcal{H}_n \otimes \mathcal{H}_n$. In this example, the multifractional integration of SPHARMA(1,1) process generated in Section 5.1 has been achieved in terms of LRD operator \mathcal{A} having eigenvalues displayed at the left-hand side of Figure 8 in Section D.1.4 of the Appendices, with $L_\alpha = 0.9982$ and $l_\alpha = 0.3041$, and \mathcal{H}_8 being the dominant subspace. The same functional sample sizes as in Examples 1–3 have been

Table 2: **Example 4.** $\|\mathcal{S}_{B_T}\|_{\mathcal{S}(L^2(\mathbb{M}_d, d\nu, \mathbb{C}))}$, of \mathcal{S}_{B_T} projected into $\bigoplus_{n=1}^8 \mathcal{H}_n \otimes \mathcal{H}_n$ ($\beta = 1/4$, $L_\alpha = 0.9982$ and $l_\alpha = 0.3041$)

Sample Size	1000	5000	10000	30000	50000	100000
	6.5651e+05	3.8623e+07	2.2172e+08	3.5383e+09	1.2688e+10	7.2258e+10

considered. One can observe, in the three plots displayed at the right-hand side of Figure 8 in Section D.1.4 of the Appendices, that the decreasing patterns over $n = 1, \dots, 8$, displayed in Figures 2, 4 and 6 (see Sections D.1.1–D.1.3 of the Appendices) do not hold in this example. Table 2 also illustrates a faster increasing than in Examples 1–3 of $\|\mathcal{S}_{B_T}\|_{\mathcal{S}(L^2(\mathbb{M}_d, d\nu, \mathbb{C}))}$, for functional sample sizes ranging from 1000 to 100000, under $l_\alpha > 1/4$, and $B_T = T^{-1/4}$.

5.4 Empirical size and power analysis

The empirical size and power properties of the testing approach presented are now illustrated. We have applied the random projection methodology. Tables 3 and 4 display the numerical results for 8 random functional directions, i.e., equation (38) is implemented including $\mathbf{k}_{1,0,1,0}$, $\mathbf{k}_{1,1,1,1}$, $\mathbf{k}_{2,1,2,1}$, $\mathbf{k}_{2,2,2,2}$, $\mathbf{k}_{3,1,3,1}$, $\mathbf{k}_{3,2,3,2}$, $\mathbf{k}_{3,3,3,3}$, defined in (39). Model SPHARMA(1,1) generated in Section 5.1 has been considered in the computation of the empirical size of the test. Multifractationally integrated SPHARMA(1,1) model, generated in Section 5.2.1, defines the scenario under the alternative to compute the empirical power. For each one of the eight random directions tested, we have analyzed the functional samples sizes $T = 50, 100, 500, 1000$, and, for each functional sample size, we have considered $R = 500, 1000, 3000$ repetitions.

The empirical size properties of the proposed testing procedure are quite robust, as one can observe in the numerical results displayed in Table 3, for each one of the T values analyzed when different values of R are considered. One can also observe, in Table 4, the increasing patterns displayed by the empirical power with respect to the functional sample sizes tested in all random directions. Note that these empirical power values are in the interval $[0.776, 1]$. In particular, since the threshold $T = 1000$, the empirical power is almost 1 for any of the three values of R studied.

Table 3: *Empirical size* ($\beta = 1/4$, $\mathbf{k}_{n,j,h,l}$, $n = h = 1, 2, 3$, $\alpha = 0.05$)

R	T=50							
500	0.0280	0.0560	0.0360	0.0480	0.0600	0.0600	0.0360	0.0520
1000	0.0480	0.0420	0.0320	0.0380	0.0420	0.0440	0.0320	0.0300
3000	0.0420	0.0447	0.0453	0.0353	0.0413	0.0400	0.0440	0.0507
R	T=100							
500	0.0360	0.0680	0.0440	0.0720	0.0520	0.0240	0.0360	0.0400
1000	0.0280	0.0380	0.0380	0.0500	0.0380	0.0740	0.0340	0.0360
3000	0.0373	0.0507	0.0407	0.0460	0.0440	0.0360	0.0600	0.0480
R	T=500							
500	0.0440	0.0520	0.0320	0.0640	0.0320	0.0480	0.0320	0.0480
1000	0.0420	0.0400	0.0500	0.0460	0.0420	0.0380	0.0540	0.0240
3000	0.0453	0.0393	0.0447	0.0407	0.0427	0.0507	0.0453	0.0553
R	T=1000							
500	0.0520	0.0360	0.0400	0.0560	0.0600	0.0640	0.0480	0.0520
1000	0.0440	0.0380	0.0400	0.0580	0.0500	0.0360	0.0520	0.0400
3000	0.0573	0.0480	0.0507	0.0467	0.0440	0.0453	0.0487	0.0447

6 Final comments and discussion

The simulation study illustrates four key aspects of our approach, briefly summarized in points (i)–(iv) below:

- (i) The tight property under H_0 of the random projection sequence

$$\left\langle \sqrt{B_T T}(\widehat{\mathcal{F}}_\omega^{(T)} - E[\widehat{\mathcal{F}}_\omega^{(T)}]), S_{n,j}^d \otimes \overline{S_{h,l}^d} \right\rangle_{\mathcal{S}(L^2(\mathbb{M}_d, d\nu, \mathbb{C}))}$$

$$j = 1, \dots, \Gamma(n, d), \quad h = 1, \dots, \Gamma(h, d), \quad n, h \in \mathbb{N}_0,$$

allowing the application of Prokhorov Theorem to prove the convergence, as $T \rightarrow \infty$, of \mathcal{S}_{B_T} to $\widehat{\mathcal{F}}_0$, in the space $\mathcal{L}_{\mathcal{S}(L^2(\mathbb{M}_d, d\nu, \mathbb{C}))}^2(\Omega, \mathcal{A}, P)$. In particular, the asymptotic Gaussian distribution of \mathcal{S}_{B_T} under H_0 follows. This result is illustrated in Section 5.1 from Theorem 1.2.1 in [7].

- (ii) The crucial role played by our design of the test statistics operator in the derivation of the conditions assumed to obtain consistency of the test (see Proposition 1 and Theorem 2). The simulation study also reveals that the additional conditions assumed in Theorem 3 lead to universal a.s. divergence rates, not affected by the localization of the dominant

Table 4: *Empirical power* ($\beta = 1/4$, $\mathbf{k}_{n,j,h,l}$, $n = h = 1, 2, 3$, $\alpha = 0.05$)

R	T=50							
500	0.9200	0.9240	0.8640	0.8880	0.8480	0.8160	0.7760	0.7800
1000	0.9000	0.9000	0.8860	0.8980	0.8000	0.8320	0.7840	0.7840
3000	0.9247	0.9253	0.8713	0.8760	0.8247	0.8273	0.7980	0.8013
R	T=100							
500	0.9920	0.9920	0.9920	0.9880	0.9840	0.9800	0.9880	0.9720
1000	0.9880	0.9880	0.9860	0.9840	0.9800	0.9720	0.9740	0.9840
3000	0.9893	0.9893	0.9920	0.9827	0.9820	0.9773	0.9767	0.9747
R	T=500							
500	1.0000	1.0000	1.0000	0.9960	1.0000	0.9960	1.0000	1.0000
1000	1.0000	1.0000	1.0000	1.0000	0.9980	1.0000	0.9980	1.0000
3000	1.0000	0.9987	1.0000	1.0000	0.9993	1.0000	0.9993	0.9993
R	T=1000							
500	1	1	1	1	1	1	1	1
1000	1	1	1	1	1	1	1	1
3000	1	1	1	1	1	1	1	1

eigenspace, or the value of the parameter $\beta \in (0, 1)$ chosen, under the bandwidth parameter scenario $B_T = T^{-\beta}$ when $l_\alpha > 1/4$.

- (iii) When higher orders of singularity are displayed at zero frequency, beyond the restriction $L_\alpha < 1/2$, a faster divergence of the sample values of the Hilbert–Schmidt operator norm of \mathcal{S}_{B_T} , and of its diagonal projections, is observed.
- (iv) The testing approach adopted displays good empirical size and power properties for finite functional sample sizes, as displayed in Tables 3 and 4, where \mathcal{S}_{B_T} satisfies Carleman condition.

Regarding topic (ii), our final conclusions are also supported by the numerical results showed in Table 5, where, in the three examples analyzed, for large functional sample sizes $T = 1000, 50000, 100000$, the sample values of $\left\| \frac{\mathcal{S}_{B_T}}{(TB_T)^{1/2}} \right\|_{\mathcal{S}(L^2(\mathbb{M}_d, d\nu, \mathbb{C}))}$ are displayed, when \mathcal{S}_{B_T} is projected into $\bigoplus_{n=1}^8 \mathcal{H}_n \otimes \mathcal{H}_n$, and $\beta = 0.2, 0.55, 0.9$. Although, as expected, the sample values of $\left\| \frac{\mathcal{S}_{B_T}}{(TB_T)^{1/2}} \right\|_{\mathcal{S}(L^2(\mathbb{M}_d, d\nu, \mathbb{C}))}$ slightly increase when β increases in Examples 1–3, no significant differences are observed in the sample divergence rate of

Table 5: $\left\| \frac{\mathcal{S}_{B_T}}{(TB_T)^{1/2}} \right\|_{\mathcal{S}(L^2(\mathbb{M}_d, d\nu, \mathbb{C}))}$, \mathcal{S}_{B_T} projected into $\bigoplus_{n=1}^8 \mathcal{H}_n \otimes \mathcal{H}_n$

$B_T = T^{-\beta}$	T	Example 1	Example 2	Example 3
$\beta = 0.2$	1000	1.6885(1.0e+04)	1.6384(1.0e+04)	1.6438(1.0e+04)
	50000	4.3549(1.0e+07)	4.2251(1.0e+07)	4.2290(1.0e+07)
	100000	1.7493(1.0e+08)	1.6944(1.0e+08)	1.6989(1.0e+08)
$\beta = 0.55$	1000	1.8067 (1.0e+04)	1.7733(1.0e+04)	1.7693(1.0e+04)
	50000	4.4789(1.0e+07)	4.3747(1.0e+07)	4.3510(1.0e+07)
	100000	1.7984(1.0e+08)	1.7470(1.0e+08)	1.7476(1.0e+08)
$\beta = 0.9$	1000	2.0296(1.0e+04)	2.0109(1.0e+04)	1.9993(1.0e+04)
	50000	4.5133(1.0e+07)	4.4271(1.0e+07)	4.4138(1.0e+07)
	100000	1.8040 (1.0e+08)	1.7518(1.0e+08)	1.7624(1.0e+08)

$\left\| \frac{\mathcal{S}_{B_T}}{(TB_T)^{1/2}} \right\|_{\mathcal{S}(L^2(\mathbb{M}_d, d\nu, \mathbb{C}))}$, for the three values of parameter β analyzed in Table 5 (see the proof of Theorem 3). Furthermore, as proved in Theorem 3, under condition $l_\alpha > 1/4$, when $B_T = T^{-\beta}$, $\beta \in (0, 1)$, one can also observe that the location of the dominant eigenspace does not affect the sample divergence rate. Note also that, as illustrated in [22], the regular spectral factor \mathcal{M}_ω , corresponding here to the SPHARMA(p,q) functional spectrum, has not effect in the asymptotic analysis when its multifractionally integration is considered.

Finally, we remark that all computations involved in the simulation study undertaken, in particular, in the implementation of the proposed inference tools and testing approach, have been achieved in terms of a unique orthonormal basis, given by the eigenfunctions of the Laplace Beltrami operator. Thus, we have worked under the scenario where the eigenfunctions of the elements of the covariance and spectral density operator families are known. This fact constitutes an important advantage of the analyzed setting, avoiding the use of empirical eigenfunction bases. We have also worked under the context of fully observed functional data. Under a manifold random uniform sampling design, the case of sparse discretely observed functional data can be addressed in a similar way, computing projections via numerical Monte–Carlo integration (see, e.g., [40]).

Acknowledgements

This work has been supported in part by projects PID2022–142900NB-I00 and PID2020-116587GB-I00, financed by MCIU/AEI/10.13039/501100011033 and by FEDER UE, and CEX2020-001105-M MCIN/AEI/10.13039/501100011033), as well as supported by grant ED431C 2021/24 (Grupos competitivos) financed

by Xunta de Galicia through European Regional Development Funds (ERDF).

Appendices

The proofs of the results of the paper are given in the subsequent sections.

A Proofs for Section 2

A.1 Proof of Theorem 2.2

Proof. From Lemma 2.1,

$$\sqrt{B_T T}(\widehat{f}_{\omega_j}^{(T)} - E[\widehat{f}_{\omega_j}^{(T)}]) \rightarrow_D \widehat{f}_{\omega_j}, \quad j = 1, \dots, J, \quad (44)$$

where \rightarrow_D denotes the convergence in distribution. Here, \widehat{f}_{ω_j} , $j = 1, \dots, J$, are jointly zero-mean complex Gaussian elements in $\mathcal{S}(L^2(\mathbb{M}_d, d\nu, \mathbb{C})) \equiv L^2(\mathbb{M}_d^2, d\nu \otimes d\nu, \mathbb{C})$, with covariance kernel:

$$\begin{aligned} \text{cov}(\widehat{f}_{\omega_i}(x_1, y_1), \widehat{f}_{\omega_j}(x_2, y_2)) &= 2\pi \|W\|_{L^2(\mathbb{R})}^2 \{ \eta(\omega_i - \omega_j) f_{\omega_i}(x_1, x_2) f_{-\omega_i}(y_1, y_2) \\ &\quad + \eta(\omega_i + \omega_j) f_{\omega_i}(x_1, y_2) f_{-\omega_i}(y_1, x_2) \}, \quad (x_i, y_i) \in \mathbb{M}_d^2, \quad i = 1, 2, \end{aligned} \quad (45)$$

with $\eta(\omega) = 1$, for $\omega \in 2\pi\mathbb{Z}$, and $\eta(\omega) = 0$, otherwise.

Let us consider $\{S_{n,j}^d, \quad j = 1, \dots, \Gamma(n, d), \quad n \in \mathbb{N}_0\}$, the orthonormal basis of eigenfunctions of the Laplace-Beltrami operator Δ_d on $L^2(\mathbb{M}_d, d\nu, \mathbb{C})$. From equation (45), applying invariance property leading to

$$f_\omega(\tau, \sigma) \underset{\mathcal{S}(L^2(\mathbb{M}_d, d\nu, \mathbb{C}))}{=} \sum_{n \in \mathbb{N}_0} f_n(\omega) \sum_{j=1}^{\Gamma(n, d)} S_{n,j}^d \otimes \overline{S_{n,j}^d}(\tau, \sigma), \quad (\tau, \sigma) \in \mathbb{M}_d^2, \quad (46)$$

we obtain, for $\tau_1, \sigma_1, \tau_2, \sigma_2 \in \mathbb{M}_d$,

$$\begin{aligned} \text{cov}(\widehat{f}_\omega(\tau_1, \sigma_1), \widehat{f}_\omega(\tau_2, \sigma_2)) &= 2\pi \|W\|_{L^2(\mathbb{R})}^2 \\ &\times \left[\sum_{n, h \in \mathbb{N}_0} \sum_{j=1}^{\Gamma(n, d)} \sum_{l=1}^{\Gamma(h, d)} f_n(\omega) f_h(\omega) S_{n,j}^d(\tau_1) \overline{S_{h,l}^d(\sigma_1)} \overline{S_{n,j}^d(\tau_2)} S_{h,l}^d(\sigma_2) \right. \\ &\quad \left. + \eta(2\omega) \sum_{n, h \in \mathbb{N}_0} \sum_{j=1}^{\Gamma(n, d)} \sum_{l=1}^{\Gamma(h, d)} f_n(\omega) f_h(\omega) S_{n,j}^d(\tau_1) \overline{S_{h,l}^d(\sigma_1)} S_{h,l}^d(\tau_2) \overline{S_{n,j}^d(\sigma_2)} \right]. \end{aligned} \quad (47)$$

Under H_0 , from Theorem D2 in the Supplementary Material of [24], keeping in mind (46),

$$\begin{aligned}
& \text{cov} \left(\widehat{f}_\omega^{(T)}(\tau_1, \sigma_1), \widehat{f}_\omega^{(T)}(\tau_2, \sigma_2) \right) \\
&= \frac{2\pi}{T} \int_{-\pi}^{\pi} W^{(T)}(\omega - \alpha) W^{(T)}(\omega - \alpha) f_\alpha(\tau_1, \tau_2) \overline{f_\alpha(\sigma_1, \sigma_2)} d\alpha \\
&+ \frac{2\pi}{T} \int_{-\pi}^{\pi} W^{(T)}(\omega - \alpha) W^{(T)}(\omega + \alpha) f_\alpha(\tau_1, \sigma_2) \overline{f_\alpha(\sigma_1, \tau_2)} d\alpha \\
&+ \mathcal{O}(B_T^{-2} T^{-2}) + \mathcal{O}(T^{-1}) \\
&= \frac{2\pi}{T} \sum_{n, h \in \mathbb{N}_0} \sum_{j=1}^{\Gamma(n, d)} \sum_{l=1}^{\Gamma(h, d)} \int_{-\pi}^{\pi} W^{(T)}(\omega - \alpha) W^{(T)}(\omega - \alpha) f_n(\alpha) f_h(\alpha) d\alpha \\
&\quad \times S_{n,j}^d(\tau_1) \overline{S_{h,l}^d(\sigma_1)} \overline{S_{n,j}^d(\tau_2)} S_{h,l}^d(\sigma_2) \\
&\quad + \frac{2\pi}{T} \int_{-\pi}^{\pi} W^{(T)}(\omega - \alpha) W^{(T)}(\omega + \alpha) f_n(\alpha) f_h(\alpha) d\alpha \\
&\quad \times S_{n,j}^d(\tau_1) \overline{S_{h,l}^d(\sigma_1)} S_{h,l}^d(\tau_2) \overline{S_{n,j}^d(\sigma_2)} + \mathcal{O}(B_T^{-2} T^{-2}) + \mathcal{O}(T^{-1}). \tag{48}
\end{aligned}$$

From (48), applying Cauchy–Schwartz inequality, and the orthonormality of the basis of eigenfunctions of the Laplace Beltrami operator, the following inequalities hold: For every $j = 1, \dots, \Gamma(n, d)$, $n \in \mathbb{N}_0$, and $l = 1, \dots, \Gamma(h, d)$, $h \in \mathbb{N}_0$, and for certain positive constants \mathcal{N}_1 , $\varepsilon > 0$,

$$\begin{aligned}
& E \left[\left| \left\langle \sqrt{B_T T} (\widehat{\mathcal{F}}_\omega^{(T)} - E[\widehat{\mathcal{F}}_\omega^{(T)}]), S_{n,j}^d \otimes \overline{S_{h,l}^d} \right\rangle_{\mathcal{S}(L^2(\mathbb{M}_d, d\nu, \mathbb{C}))} \right|^2 \right] \\
&= 2\pi \int_{-\pi}^{\pi} W \left(\frac{\omega - \alpha}{B_T} \right) \left[W \left(\frac{\omega - \alpha}{B_T} \right) + W \left(\frac{\omega + \alpha}{B_T} \right) \right] \left\langle S_{n,j}^d, \overline{S_{h,l}^d} \right\rangle_{L^2(\mathbb{M}_d, d\nu, \mathbb{C})} \\
&\quad \times \left\langle \overline{S_{n,j}^d}, S_{h,l}^d \right\rangle_{L^2(\mathbb{M}_d, d\nu, \mathbb{C})} \left[f_n(\alpha) f_h(\alpha) \frac{d\alpha}{B_T} + \mathcal{O}(B_T^{-2} T^{-2}) + \mathcal{O}(T^{-1}) \right] \\
&\leq 2\pi \int_{-\pi}^{\pi} W \left(\frac{\omega - \alpha}{B_T} \right) \left[W \left(\frac{\omega - \alpha}{B_T} \right) + W \left(\frac{\omega + \alpha}{B_T} \right) \right] f_n(\alpha) f_h(\alpha) \frac{d\alpha}{B_T} \\
&\quad + \mathcal{O}(B_T^{-2} T^{-2}) + \mathcal{O}(T^{-1}) \leq \mathcal{N}_1 \left[\sum_{\tau \in \mathbb{Z}} \|\mathcal{R}_\tau\|_{L^1(L^2(\mathbb{M}_d, d\nu, \mathbb{C}))} \right]^2 + \varepsilon < \infty, \tag{49}
\end{aligned}$$

under SRD, where $\widehat{\mathcal{F}}_\omega^{(T)}$ denotes the weighted periodogram operator with kernel $\widehat{f}_\omega^{(T)}$. In equation (49), we have considered T sufficiently large to apply the identity $W(x) = 1/B_T W(x/B_T)$, for $B_T < 1$, and $x \in [-\pi, \pi]$ (see

Lemma F11 of the Supplementary Material in [24]). Thus, under H_0 , assuming the conditions in Lemma 2.1, the sequence $\sqrt{B_T T}(\widehat{\mathcal{F}}_\omega^{(T)} - E[\widehat{\mathcal{F}}_\omega^{(T)}])$ is tight. Hence, the convergence, as $T \rightarrow \infty$, of $\sqrt{B_T T}(\widehat{\mathcal{F}}_\omega^{(T)} - E[\widehat{\mathcal{F}}_\omega^{(T)}])$ to the Gaussian random operator $\widehat{\mathcal{F}}_\omega$ with kernel \widehat{f}_ω (see equation 44), in the norm of the space $\mathcal{L}_{\mathcal{S}(L^2(\mathbb{M}_d, d\nu; \mathbb{C}))}^2(\Omega, \mathcal{A}, P)$, follows from Prokhorov Theorem. Here, $\mathcal{L}_{\mathcal{S}(L^2(\mathbb{M}_d, d\nu; \mathbb{C}))}^2(\Omega, \mathcal{A}, P)$ denotes the space of zero-mean second-order $\mathcal{S}(L^2(\mathbb{M}_d, d\nu; \mathbb{C}))$ -valued random variables with the norm $\sqrt{E\|\cdot\|_{\mathcal{S}(L^2(\mathbb{M}_d, d\nu; \mathbb{C}))}^2}$.

Let us now compute

$$\begin{aligned}
& E \left\| (\mathcal{S}_{B_T} - E[\mathcal{S}_{B_T}]) - \widehat{\mathcal{F}}_0 \right\|_{\mathcal{S}(L^2(\mathbb{M}_d, d\nu; \mathbb{C}))}^2 \\
&= \sum_{n, h \in \mathbb{N}_0} \sum_{j=1}^{\Gamma(n, d)} \sum_{l=1}^{\Gamma(h, d)} E \left| (\mathcal{S}_{B_T} - E[\mathcal{S}_{B_T}]) (\overline{S_{h,l}^d})(S_{n,j}^d) - \widehat{\mathcal{F}}_0 (\overline{S_{h,l}^d})(S_{n,j}^d) \right|^2 \\
&= \int_{\left[-\frac{\sqrt{B_T}}{2}, \frac{\sqrt{B_T}}{2}\right]^2} \left\| \text{Cov} \left(\sqrt{TB_T} \widehat{\mathcal{F}}_\omega^{(T)} - \widehat{\mathcal{F}}_0, \sqrt{TB_T} \widehat{\mathcal{F}}_\xi^{(T)} - \widehat{\mathcal{F}}_0 \right) \right\|_{L^1(\mathcal{S}(L^2(\mathbb{M}_d, d\nu; \mathbb{C})))} d\omega d\xi, \tag{50}
\end{aligned}$$

where, as before, $\widehat{\mathcal{F}}_0$ is the Gaussian random element with random kernel \widehat{f}_0 introduced in equation (44). Here, $\|\cdot\|_{L^1(\mathcal{S}(L^2(\mathbb{M}_d, d\nu; \mathbb{C})))}$ denotes the trace norm in the space of nuclear operators on $\mathcal{S}(L^2(\mathbb{M}_d, d\nu; \mathbb{C}))$. That is,

$$\begin{aligned}
& \left\| \text{Cov} \left(\sqrt{TB_T} \widehat{\mathcal{F}}_\omega^{(T)} - \widehat{\mathcal{F}}_0, \sqrt{TB_T} \widehat{\mathcal{F}}_\xi^{(T)} - \widehat{\mathcal{F}}_0 \right) \right\|_{L^1(\mathcal{S}(L^2(\mathbb{M}_d, d\nu; \mathbb{C})))} \\
&= \sum_{n, h, j, l} \text{Cov} \left(\sqrt{TB_T} \widehat{\mathcal{F}}_\omega^{(T)} - \widehat{\mathcal{F}}_0, \sqrt{TB_T} \widehat{\mathcal{F}}_\xi^{(T)} - \widehat{\mathcal{F}}_0 \right) \left(S_{n,j}^d \otimes \overline{S_{h,l}^d} \right) \left(S_{n,j}^d \otimes \overline{S_{h,l}^d} \right), \tag{51}
\end{aligned}$$

where for a bounded linear operator \mathcal{A} on a separable Hilbert space H , $\mathcal{A}(\varphi)(\phi) = \langle \mathcal{A}(\varphi), \phi \rangle_H$, for every $\varphi, \phi \in \text{Dom}(\mathcal{A})$.

In a similar way to equation (49), from equations (47) and (48), applying Cauchy–Schwartz inequality in $\mathcal{L}^2(\Omega, \mathcal{A}, P)$, the space of complex-valued zero-mean second-order random variables on (Ω, \mathcal{A}, P) , and in $L^2(\mathbb{M}_d, d\nu; \mathbb{C})$,

$$\begin{aligned}
& \int_{-\pi}^{\pi} E \left\| \sqrt{TB_T} \left(\widehat{\mathcal{F}}_\omega^{(T)} - E \left[\widehat{\mathcal{F}}_\omega^{(T)} \right] \right) - \widehat{\mathcal{F}}_0 \right\|_{\mathcal{S}(L^2(\mathbb{M}_d, d\nu; \mathbb{C}))}^2 d\omega \\
& \leq \mathcal{N}_2 \left[\left(\sum_{\tau \in \mathbb{Z}} \|\mathcal{R}_\tau\|_{L^1(L^2(\mathbb{M}_d, d\nu; \mathbb{C}))} \right)^2 + \left(\sum_{\tau \in \mathbb{Z}} \|\mathcal{R}_\tau\|_{L^1(L^2(\mathbb{M}_d, d\nu; \mathbb{C}))} \right)^4 \right] < \infty, \tag{52}
\end{aligned}$$

under H_0 , for certain positive constant \mathcal{N}_2 .

Note that $\delta_T(0 - \omega) = \delta_T(\omega) = \mathbb{I}_{[-\sqrt{B_T}/2, \sqrt{B_T}/2]}(\omega)/\sqrt{B_T}$ behaves as a truncated Dirac Delta distribution at point zero, i.e., $\delta_T(\omega) \rightarrow 0$, for $\omega \neq 0$, and $\delta_T(0) \rightarrow \infty$, as $T \rightarrow \infty$ (see, e.g., [12]). Equivalently, for every $g \in L^2([-\pi, \pi])$,

$$\int_{[-\sqrt{B_T}/2, \sqrt{B_T}/2]} g(\omega) \frac{d\omega}{\sqrt{B_T}} = \int_{[-\pi, \pi]} \delta_T(\omega) g(\omega) d\omega \rightarrow g(0), \quad T \rightarrow \infty, \quad (53)$$

where $L^2([-\pi, \pi])$ denotes, as usual, the space of square integrable functions on the interval $[-\pi, \pi]$.

From equations (50)–(53), applying Dominated Convergence Theorem,

$$\begin{aligned} & \lim_{T \rightarrow \infty} E \left\| (\mathcal{S}_{B_T} - E[\mathcal{S}_{B_T}]) - \hat{\mathcal{F}}_0 \right\|_{\mathcal{S}(L^2(\mathbb{M}_d, d\nu, \mathbb{C}))}^2 \\ &= \lim_{T \rightarrow \infty} \sum_{n, h \in \mathbb{N}_0} \sum_{j=1}^{\Gamma(n, d)} \sum_{l=1}^{\Gamma(h, d)} \int_{[-\pi, \pi]^2} \delta_T(0 - \omega) \delta_T(0 - \xi) \\ & \quad \times \text{Cov} \left(\sqrt{TB_T} \hat{\mathcal{F}}_\omega^{(T)} - \hat{\mathcal{F}}_0, \sqrt{TB_T} \hat{\mathcal{F}}_\xi^{(T)} - \hat{\mathcal{F}}_0 \right) \left(S_{n, j}^d \otimes \overline{S_{h, l}^d} \right) \left(S_{n, j}^d \otimes \overline{S_{h, l}^d} \right) d\omega d\xi \\ &= \sum_{n, h \in \mathbb{N}_0} \sum_{j=1}^{\Gamma(n, d)} \sum_{l=1}^{\Gamma(h, d)} \lim_{T \rightarrow \infty} \int_{[-\pi, \pi]^2} \delta_T(0 - \omega) \delta_T(0 - \xi) \\ & \quad \times \text{Cov} \left(\sqrt{TB_T} \hat{\mathcal{F}}_\omega^{(T)} - \hat{\mathcal{F}}_0, \sqrt{TB_T} \hat{\mathcal{F}}_\xi^{(T)} - \hat{\mathcal{F}}_0 \right) \left(S_{n, j}^d \otimes \overline{S_{h, l}^d} \right) \left(S_{n, j}^d \otimes \overline{S_{h, l}^d} \right) d\omega d\xi = 0, \end{aligned} \quad (54)$$

in view of the convergence in $\mathcal{L}_{\mathcal{S}(L^2(\mathbb{M}_d, d\nu, \mathbb{C}))}^2(\Omega, \mathcal{A}, P)$ of $\sqrt{TB_T} \left(\hat{\mathcal{F}}_0^{(T)} - E \left[\hat{\mathcal{F}}_0^{(T)} \right] \right)$ to $\hat{\mathcal{F}}_0$. Thus, the convergence in distribution of $\mathcal{S}_{B_T} - E[\mathcal{S}_{B_T}]$ to $\hat{\mathcal{F}}_0$ holds.

B Proofs for Section 3

B.1 Proof of Lemma 3.1

Proof. Let us consider

$$\begin{aligned} & \left\| \int_{-\pi}^{\pi} [\mathcal{F}_\omega - \mathcal{F}_\omega^{(T)}] d\omega \right\|_{\mathcal{S}(L^2(\mathbb{M}_d, d\nu, \mathbb{C}))}^2 \\ &= \sum_{n \in \mathbb{N}_0} \sum_{j=1}^{\Gamma(n, d)} \int_{[-\pi, \pi]^2} [f_n(\omega) - f_n^{(T)}(\omega)] \overline{f_n(\xi)} d\xi d\omega \\ & \quad + \int_{[-\pi, \pi]^2} [f_n^{(T)}(\omega) - f_n(\omega)] \overline{f_n^{(T)}(\xi)} d\xi d\omega, \end{aligned} \quad (55)$$

where the sequence of functions

$$f_n^{(T)}(\omega) = \int_{-\pi}^{\pi} F_T(\omega - \xi) f_n(\xi) d\xi, \quad \forall \omega \in [-\pi, \pi], \quad n \in \mathbb{N}_0,$$

defines the frequency-varying pure point spectra of the operator family $\left\{ \mathcal{F}_\omega^{(T)} = E_{H_1} \left[\mathcal{P}_\omega^{(T)} \right], \omega \in [-\pi, \pi] \right\}$, for every $T \geq 2$, with $\mathcal{P}_\omega^{(T)}$ denoting the periodogram operator, and E_{H_1} the expectation under the alternative H_1 .

Under H_1 , for every $n \in \mathbb{N}_0$, $f_n(\cdot) \in L^1([-\pi, \pi])$. Applying well-known properties of Féjer kernel, we then obtain, as $T \rightarrow \infty$,

$$f_n^{(T)}(\omega) \rightarrow f_n(\omega), \quad \forall \omega \in [-\pi, \pi] \setminus \Lambda_0, \quad \text{with} \quad \int_{\Lambda_0} d\omega = 0. \quad (56)$$

From Young convolution inequality in $L^2([-\pi, \pi])$, for each $n \in \mathbb{N}_0$, and $T \geq 2$,

$$\int_{[-\pi, \pi]} |f_n^{(T)}(\omega)|^2 d\omega \leq \int_{[-\pi, \pi]} |f_n(\omega)|^2 d\omega < \infty, \quad (57)$$

under H_1 , since $l_\alpha, L_\alpha \in (0, 1/2)$. Thus, $f_n^{(T)} \in L^2([-\pi, \pi])$, for every $n \in \mathbb{N}_0$, and T .

To apply Dominated Convergence Theorem in (55), the following additional inequalities are considered, obtained from triangle inequality, Young convolution inequality for functions in $L^1([-\pi, \pi])$, and Jensen's inequality, keeping in mind that $f_n(\omega) \geq 0$, a.s. in $\omega \in [-\pi, \pi]$, for every $n \in \mathbb{N}_0$,

$$\begin{aligned} \left| \int_{[-\pi, \pi]^2} \overline{f_n^{(T)}(\xi)} f_n^{(T)}(\omega) d\xi d\omega \right| &\leq \int_{[-\pi, \pi]^2} \left| \overline{f_n^{(T)}(\xi)} f_n^{(T)}(\omega) \right| d\xi d\omega \\ &\leq \int_{[-\pi, \pi]^2} |f_n(\xi) f_n(\omega)| d\xi d\omega = \left[\int_{[-\pi, \pi]} f_n(\omega) d\omega \right]^2 \leq \int_{[-\pi, \pi]} |f_n(\omega)|^2 d\omega. \end{aligned} \quad (58)$$

Also, in a similar way,

$$\begin{aligned} \left| \int_{[-\pi, \pi]^2} \overline{f_n^{(T)}(\xi)} f_n(\omega) d\xi d\omega \right| &\leq \int_{[-\pi, \pi]} |f_n(\omega)|^2 d\omega \\ \left| \int_{[-\pi, \pi]^2} \overline{f_n(\xi)} f_n^{(T)}(\omega) d\xi d\omega \right| &\leq \int_{[-\pi, \pi]} |f_n(\omega)|^2 d\omega \\ \left| \int_{[-\pi, \pi]^2} f_n(\xi) f_n(\omega) d\xi d\omega \right| &\leq \int_{[-\pi, \pi]} |f_n(\omega)|^2 d\omega. \end{aligned} \quad (59)$$

Under H_1 ,

$$\sum_{n \in \mathbb{N}_0} \Gamma(n, d) \int_{[-\pi, \pi]} |f_n(\omega)|^2 d\omega = \int_{[-\pi, \pi]} \|\mathcal{F}_\omega\|_{\mathcal{S}(L^2(\mathbb{M}_d, d\nu, \mathbb{C}))}^2 d\omega < \infty. \quad (60)$$

From equations (56)–(60), one can apply Dominated Convergence Theorem in equation (55), obtaining

$$\begin{aligned} & \lim_{T \rightarrow \infty} \left\| \int_{-\pi}^{\pi} [\mathcal{F}_\omega - \mathcal{F}_\omega^{(T)}] d\omega \right\|_{\mathcal{S}(L^2(\mathbb{M}_d, d\nu, \mathbb{C}))}^2 \\ &= \sum_{n \in \mathbb{N}_0} \sum_{j=1}^{\Gamma(n, d)} \int_{[-\pi, \pi]^2} \lim_{T \rightarrow \infty} \overline{f_n^{(T)}(\xi)} [f_n^{(T)}(\omega) - f_n(\omega)] d\xi d\omega \\ &+ \int_{[-\pi, \pi]^2} \lim_{T \rightarrow \infty} \overline{f_n(\xi)} [f_n(\omega) - f_n^{(T)}(\omega)] d\xi d\omega = 0. \end{aligned} \quad (61)$$

The rate of convergence to zero of the bias is now obtained in the time domain. Let B_n be defined as

$$B_n(t) = \int_{-\pi}^{\pi} \exp(it\omega) f_n(\omega) d\omega, \quad t \in \mathbb{Z}, \quad n \in \mathbb{N}_0. \quad (62)$$

The function sequence

$$\left\{ \mathbb{I}_{[-(T-1), T-1]}(t) \frac{T-|t|}{T} B_n(t), \quad t \in \mathbb{Z}, \quad n \in \mathbb{N}_0 \right\}_{T \geq 2}$$

pointwise converges, as $T \rightarrow \infty$, to $B_n(t)$ with rate of convergence T^{-1} , and satisfies, for every $T \geq 2$,

$$\left| \mathbb{I}_{[-(T-1), T-1]}(t) \frac{T-|t|}{T} B_n(t) \right|^2 \leq |B_n(t)|^2. \quad (63)$$

From (60) and Parseval identity,

$$\begin{aligned} & \sum_{t \in \mathbb{Z}} \sum_{n \in \mathbb{N}_0} \Gamma(n, d) |B_n(t)|^2 = \sum_{t \in \mathbb{Z}} \|\mathcal{R}_t\|_{\mathcal{S}(L^2(\mathbb{M}_d, d\nu, \mathbb{C}))}^2 \\ &= \int_{-\pi}^{\pi} \|\mathcal{F}_\omega\|_{\mathcal{S}(L^2(\mathbb{M}_d, d\nu, \mathbb{C}))}^2 d\omega < \infty. \end{aligned} \quad (64)$$

From equations (63) and (64), Dominated Convergence Theorem then leads to

$$\begin{aligned} & \lim_{T \rightarrow \infty} \sum_{t \in \mathbb{Z}} \left\| \mathcal{R}_t - \mathbb{I}_{[-(T-1), T-1]}(t) \frac{T-|t|}{T} \mathcal{R}_t \right\|_{\mathcal{S}(L^2(\mathbb{M}_d, d\nu, \mathbb{C}))}^2 \\ &= \sum_{t \in \mathbb{Z}} \sum_{n \in \mathbb{N}_0} \Gamma(n, d) \lim_{T \rightarrow \infty} \left| B_n(t) - \mathbb{I}_{[-(T-1), T-1]}(t) \frac{T-|t|}{T} B_n(t) \right|^2 = 0, \end{aligned} \quad (65)$$

and $\sum_{t \in \mathbb{Z}} \left\| \mathcal{R}_t - \mathbb{I}_{[-(T-1), T-1]}(t) \frac{T-|t|}{T} \mathcal{R}_t \right\|_{\mathcal{S}(L^2(\mathbb{M}_d, d\nu, \mathbb{C}))}^2 = \mathcal{O}(T^{-2})$. Hence, the desired result follows from Parseval identity.

B.2 Proof of Corollary 3.2

Proof.

Applying Lemma 3.1, and Lemmas F10 and F12 of Appendix F in the Supplementary Material of [24],

$$\begin{aligned} \int_{-\pi}^{\pi} E_{H_1}[\widehat{\mathcal{F}}_{\omega}^{(T)}] d\omega & \underset{\mathcal{S}(L^2(\mathbb{M}_d, d\nu, \mathbb{C}))}{=} \int_{\mathbb{R}} W(\xi) \int_{-\pi}^{\pi} [\mathcal{F}_{\omega-\xi B_T} + \mathcal{O}(T^{-1})] d\omega d\xi \\ & + \mathcal{O}(B_T^{-1} T^{-1}) \underset{\mathcal{S}(L^2(\mathbb{M}_d, d\nu, \mathbb{C}))}{=} \int_{-\pi}^{\pi} \int_{\mathbb{R}} W(\xi) \mathcal{F}_{\omega-\xi B_T} d\xi d\omega + \mathcal{O}(T^{-1}) + \mathcal{O}(B_T^{-1} T^{-1}), \end{aligned} \quad (66)$$

as we wanted to prove.

B.3 Proof of Lemma 3.3

Proof.

Under *Assumption I*, there exists an orthonormal basis $\{\phi_n, n \in \mathbb{N}\}$ of $L^2(\mathbb{M}_d^2, \otimes_{i=1}^2 \nu(dx_i), \mathbb{R})$ such that (see [14])

$$\begin{aligned} & \int_{\mathbb{M}_d} \text{cum}(X_{u_1}, X_{u_2}, X_{u_3}, X_0)(\tau_1, \tau_2, \tau_3, \tau_4) \phi_n(\tau_3, \tau_4) \nu(d\tau_3) \nu(d\tau_4) \\ & = B_n(u_1, u_2, u_3) \phi_n(\tau_1, \tau_2), \quad \forall (\tau_1, \tau_2) \in \mathbb{M}_d \times \mathbb{M}_d, \quad u_1, u_2, u_3 \in \mathbb{Z}, \quad n \geq 1. \end{aligned} \quad (67)$$

Furthermore,

$$\begin{aligned} & \int_{[-\pi, \pi]^3} \text{cum}\left(\widetilde{X}_{\omega_1}^{(T)}(\tau_1), \widetilde{X}_{\omega_2}^{(T)}(\tau_2), \widetilde{X}_{\omega_3}^{(T)}(\tau_3), \widetilde{X}_{\omega_4}^{(T)}(\tau_4)\right) d\omega_1 d\omega_2 d\omega_3 \\ & \underset{\mathcal{S}(L^2(\mathbb{M}_d^2, \otimes_{i=1}^2 \nu(dx_i), \mathbb{C}))}{=} \frac{1}{(2\pi T)^2} \int_{[-\pi, \pi]^3} \sum_{t_1, t_2, t_3, t_4=0}^{T-1} \exp\left(-i \sum_{j=1}^3 (t_j - t_4) \omega_j\right) \end{aligned}$$

$$\begin{aligned}
& \times \exp \left(-it_4 \sum_{j=1}^4 \omega_j \right) \text{cum} (X_{t_1-t_4}(\tau_1), X_{t_2-t_4}(\tau_2), X_{t_3-t_4}(\tau_3), X_0(\tau_4)) \prod_{j=1}^3 d\omega_j \\
& \stackrel{=}{=} \mathcal{S}(L^2(\mathbb{M}_d^2, \otimes_{i=1}^2 \nu(dx_i), \mathbb{C})) \int_{[-\pi, \pi]^3} \frac{1}{(2\pi T)^2} \sum_{u_1, u_2, u_3 = -(T-1)}^{T-1} \exp \left(-i \sum_{j=1}^3 u_j \omega_j \right) \\
& \quad \times \text{cum} (X_{u_1}(\tau_1), X_{u_2}(\tau_2), X_{u_3}(\tau_3), X_0(\tau_4)) \\
& \times \sum_{t \in \mathbb{Z}} h^{(T)}(u_1 + t) h^{(T)}(u_2 + t) h^{(T)}(u_3 + t) h^{(T)}(t) \exp \left(-it \left(\sum_{j=1}^4 \omega_j \right) \right) \prod_{j=1}^3 d\omega_j,
\end{aligned} \tag{68}$$

with $h(t) = 1$, $0 \leq t \leq T$, and $h(t) = 0$, otherwise. In (68), we have considered the change of variable $u_j = t_j - t_4$, $j = 1, 2, 3$, and $t = t_4$. Denote, for every $n \geq 1$, and $(\omega_1, \omega_2, \omega_3) \in [-\pi, \pi]^3$,

$$f_n(\omega_1, \omega_2, \omega_3) = \frac{1}{(2\pi)^3} \sum_{u_1, u_2, u_3 \in \mathbb{Z}} \exp \left(-i \sum_{j=1}^3 \omega_j u_j \right) B_n(u_1, u_2, u_3),$$

where, for $u_1, u_2, u_3 \in \mathbb{Z}$, $\{B_n(u_1, u_2, u_3), n \geq 1\}$ satisfies (67). From equations (67)–(68), applying Fourier transform inversion formula, for each $n \geq 1$,

$$\begin{aligned}
& T \int_{[-\pi, \pi]^3 \times \mathbb{M}_d^4} \text{cum} \left(\tilde{X}_{\omega_1}^{(T)}(\tau_1), \tilde{X}_{\omega_2}^{(T)}(\tau_2), \tilde{X}_{\omega_3}^{(T)}(\tau_3), \tilde{X}_{\omega_4}^{(T)}(\tau_4) \right) \\
& \quad \times \phi_n(\tau_1, \tau_2) \phi_n(\tau_3, \tau_4) \prod_{j=1}^4 d\tau_j \prod_{i=1}^3 d\omega_i \\
& = \frac{(2\pi)^3}{(2\pi)^2 T} \int_{[-\pi, \pi]^6} \sum_{u_1, u_2, u_3 = -(T-1)}^{T-1} \exp \left(-i \sum_{j=1}^3 u_j (\omega_j - \xi_j) \right) \\
& \times \sum_{t \in \mathbb{Z}} h^{(T)}(u_1 + t) h^{(T)}(u_2 + t) h^{(T)}(u_3 + t) h^{(T)}(t) \exp \left(-it \left(\sum_{j=1}^4 \omega_j \right) \right) \\
& \quad \times f_n(\xi_1, \xi_2, \xi_3) \prod_{j=1}^3 d\xi_j \prod_{i=1}^3 d\omega_i
\end{aligned}$$

$$\begin{aligned}
&= \frac{2\pi}{T} \int_{[-\pi, \pi]^6} \left[\sum_{u_1, u_2, u_3 = -(T-1)}^{T-1} \exp \left(-i \sum_{j=1}^3 u_j (\omega_j - \xi_j) \right) \right. \\
&\quad \times \left. \sum_{t \in \mathbb{Z}} \exp \left(-it \left(\sum_{j=1}^4 \omega_j \right) \right) h \left(t + \max_{j=1,2,3} |u_j| \right) \right] f_n(\xi_1, \xi_2, \xi_3) \prod_{j=1}^3 d\xi_j \prod_{i=1}^3 d\omega_i.
\end{aligned} \tag{69}$$

As $T \rightarrow \infty$, uniformly in $\omega_4 \in [-\pi, \pi]$,

$$\begin{aligned}
&\frac{1}{T} \left[\sum_{u_1, u_2, u_3 = -(T-1)}^{T-1} \exp \left(-i \sum_{j=1}^3 u_j (\omega_j - \xi_j) \right) \right. \\
&\quad \times \left. \sum_{t \in \mathbb{Z}} \exp \left(-it \left(\sum_{j=1}^4 \omega_j \right) \right) h \left(t + \max_{j=1,2,3} |u_j| \right) \right] \rightarrow \delta(\boldsymbol{\omega} - \boldsymbol{\xi}),
\end{aligned} \tag{70}$$

where $\delta(\boldsymbol{\omega} - \boldsymbol{\xi}) = \prod_{j=1}^3 \delta(\omega_j - \xi_j)$ denotes the Dirac Delta distribution, defining the kernel of the identity operator on $L^2([-\pi, \pi]^3)$. Using the notation

$$\begin{aligned}
\delta_T(\boldsymbol{\omega} - \boldsymbol{\xi}) &:= \frac{1}{T} \left[\sum_{u_1, u_2, u_3 = -(T-1)}^{T-1} \exp \left(-i \sum_{j=1}^3 u_j (\omega_j - \xi_j) \right) \right. \\
&\quad \times \left. \sum_{t \in \mathbb{Z}} \exp \left(-it \left(\sum_{j=1}^4 \omega_j \right) \right) h \left(t + \max_{j=1,2,3} |u_j| \right) \right] \tag{71}
\end{aligned}$$

equation (69) can be rewritten as

$$\begin{aligned}
&T \int_{[-\pi, \pi]^3 \times \mathbb{M}_d^4} \text{cum} \left(\tilde{X}_{\omega_1}^{(T)}(\tau_1), \tilde{X}_{\omega_2}^{(T)}(\tau_2), \tilde{X}_{\omega_3}^{(T)}(\tau_3), \tilde{X}_{\omega_4}^{(T)}(\tau_4) \right) \\
&\quad \times \phi_n(\tau_1, \tau_2) \phi_n(\tau_3, \tau_4) \prod_{j=1}^4 d\tau_j \prod_{i=1}^3 d\omega_i \\
&= 2\pi \int_{[-\pi, \pi]^6} \delta_T(\boldsymbol{\omega} - \boldsymbol{\xi}) f_n(\boldsymbol{\xi}) d\boldsymbol{\xi} d\boldsymbol{\omega}, \quad n \geq 1.
\end{aligned} \tag{72}$$

Note that, for $T \geq T_0$, with T_0 sufficiently large,

$$|\delta_T(\boldsymbol{\omega} - \boldsymbol{\xi}) f_n(\boldsymbol{\xi})| \leq |f_n(\boldsymbol{\xi})|, \quad \boldsymbol{\omega} \neq \boldsymbol{\xi}, \tag{73}$$

since $\delta_T(\omega - \xi) \rightarrow 0$, $T \rightarrow \infty$, for every $(\omega, \xi) \in [-\pi, \pi]^6 \setminus \Lambda$, with $\Lambda = \{(\omega, \xi) \in [-\pi, \pi]^6; \omega = \xi\} \subset [-\pi, \pi]^6$. Under *Assumption I*, applying Parseval identity,

$$\begin{aligned}
& \sum_{n \geq 1} \int_{[-\pi, \pi]^6} |f_n(\omega_1, \omega_2, \omega_3)| \prod_{j=1}^6 d\omega_j \\
& \leq (2\pi)^3 \sum_{n \geq 1} \int_{[-\pi, \pi]^3} |f_n(\omega_1, \omega_2, \omega_3)|^2 \prod_{j=1}^3 d\omega_j \\
& = (2\pi)^3 \int_{[-\pi, \pi]^3} \|\mathcal{F}_{\omega_1, \omega_2, \omega_3}\|_{\mathcal{S}(L^2(\mathbb{M}_d^2, \otimes_{i=1}^2 \nu(dx_i), \mathbb{C}))}^2 \prod_{j=1}^3 d\omega_j \\
& = (2\pi)^3 \sum_{t_1, t_2, t_3 \in \mathbb{Z}} \|\text{cum}(X_{t_1}, X_{t_2}, X_{t_3}, X_0)\|_{L^2(\mathbb{M}_d^4, \otimes_{i=1}^4 d\nu(x_i), \mathbb{R})}^2 < \infty. \quad (74)
\end{aligned}$$

Hence, from (73)–(74), applying Dominated Convergence Theorem,

$$\begin{aligned}
& \lim_{T \rightarrow \infty} \int_{[-\pi, \pi]^6} \delta_T(\omega - \xi) f_n(\xi) d\xi d\omega \\
& = \int_{[-\pi, \pi]^6} \lim_{T \rightarrow \infty} \delta_T(\omega - \xi) f_n(\xi) d\xi d\omega \\
& = \int_{[-\pi, \pi]^3} f_n(\omega) d\omega, \quad n \geq 1. \quad (75)
\end{aligned}$$

and, as $T \rightarrow \infty$,

$$\left| \int_{[-\pi, \pi]^6} \delta_T(\omega - \xi) f_n(\xi) d\xi d\omega - \int_{[-\pi, \pi]^3} f_n(\omega) d\omega \right| = \mathcal{O}(T^{-1}). \quad (76)$$

Therefore, from (72), (74) and (76), uniformly in $\omega_4 \in [-\pi, \pi]$,

$$\begin{aligned}
& \lim_{T \rightarrow \infty} \sum_n \left| T \int_{[-\pi, \pi]^3 \times \mathbb{M}_d^4} \text{cum} \left(\tilde{X}_{\omega_1}^{(T)}(\tau_1), \tilde{X}_{\omega_2}^{(T)}(\tau_2), \tilde{X}_{\omega_3}^{(T)}(\tau_3), \tilde{X}_{\omega_4}^{(T)}(\tau_4) \right) \right. \\
& \quad \left. \times \phi_n(\tau_1, \tau_2) \phi_n(\tau_3, \tau_4) \prod_{j=1}^4 d\tau_j - 2\pi f_n(\omega_1, \omega_2, \omega_3) \prod_{i=1}^3 d\omega_i \right| = 0.
\end{aligned}$$

It then follows that, as $T \rightarrow \infty$,

$$\left\| \int_{[-\pi, \pi]^3} \left[T \text{cum} \left(\tilde{X}_{\omega_1}^{(T)}, \tilde{X}_{\omega_2}^{(T)}, \tilde{X}_{\omega_3}^{(T)}, \tilde{X}_{\omega_4}^{(T)} \right) - 2\pi \mathcal{F}_{\omega_1, \omega_2, \omega_3} \right] \prod_{j=1}^3 d\omega_j \right\|_{\mathcal{S}(L^2(\mathbb{M}_d^2, \otimes_{i=1}^2 \nu(dx_i), \mathbb{C}))} \rightarrow 0, \quad (77)$$

with

$$\begin{aligned}
& T \int_{[-\pi, \pi]^3} \text{cum} \left(\tilde{X}_{\omega_1}^{(T)}, \tilde{X}_{\omega_2}^{(T)}, \tilde{X}_{\omega_3}^{(T)}, \tilde{X}_{\omega_4}^{(T)} \right) \prod_{i=1}^3 d\omega_i \\
&= 2\pi \int_{[-\pi, \pi]^3} \mathcal{F}_{\omega_1, \omega_2, \omega_3} \prod_{j=1}^3 d\omega_j + \mathcal{O}(T^{-1}),
\end{aligned}$$

in the norm of the space $\mathcal{S}(L^2(\mathbb{M}_d^2, \otimes_{i=1}^2 \nu(dx_i), \mathbb{C}))$, where $\mathcal{F}_{\omega_1, \omega_2, \omega_3}$ denotes the cumulant spectral density operator of order 4 of X under H_1 , introduced in equation (30).

C Proofs for Section 4

C.1 Proof of Proposition 4.1

Proof. Under H_1 , we have $0 < l_\alpha \leq \alpha(n) \leq L_\alpha < 1/2$, for every $n \in \mathbb{N}_0$. From Lemma 3.1, considering T sufficiently large,

$$\begin{aligned}
& \left| \int_{[-\sqrt{B_T}/2, \sqrt{B_T}/2]} E_{H_1}[\hat{f}_n^{(T)}(\omega)] \frac{d\omega}{\sqrt{B_T}} \right| \\
&= \int_{-\pi}^{\pi} \frac{1}{B_T} \left[\int_{[-\sqrt{B_T}/2, \sqrt{B_T}/2]} W\left(\frac{\omega - \alpha}{B_T}\right) \frac{d\omega}{\sqrt{B_T}} \right] f_n^{(T)}(\alpha) d\alpha \\
&+ \mathcal{O}(B_T^{-1}T^{-1}) \\
&\simeq \frac{1}{\sqrt{B_T}} \int_{-\pi}^{\pi} \frac{1}{\sqrt{B_T}} W\left(\frac{-\alpha}{B_T}\right) f_n(\alpha) d\alpha + \mathcal{O}(B_T^{-1}T^{-1}) + \mathcal{O}(T^{-1}) \\
&\geq g(T) = \mathcal{O}(B_T^{-1/2-l_\alpha}), \quad \forall n \in \mathbb{N}_0,
\end{aligned} \tag{78}$$

where $\{\hat{f}_n^{(T)}(\omega), n \in \mathbb{N}_0\}$ and $\{f_n^{(T)}(\omega), n \in \mathbb{N}_0\}$ respectively denote the frequency varying eigenvalues of the weighted periodogram operator $\hat{\mathcal{F}}_\omega^{(T)}$ and the mean operator $\mathcal{F}_\omega^{(T)} = E[\mathcal{P}_\omega^{(T)}]$. Here, $a_T \simeq b_T$ means that the two sequences

$\{a_T, T > 0\}$ and $\{b_T, T > 0\}$ have the same limit as $T \rightarrow \infty$. From (78),

$$\begin{aligned}
& \left\| \int_{[-\sqrt{B_T}/2, \sqrt{B_T}/2]} E_{H_1}[\widehat{\mathcal{F}}_\omega^{(T)}] \frac{d\omega}{\sqrt{B_T}} \right\|_{\mathcal{S}(L^2(\mathbb{M}_d, d\nu, \mathbb{C}))} \\
& \geq \left\| \int_{[-\sqrt{B_T}/2, \sqrt{B_T}/2]} E_{H_1}[\widehat{\mathcal{F}}_\omega^{(T)}] \frac{d\omega}{\sqrt{B_T}} \right\|_{\mathcal{L}(L^2(\mathbb{M}_d, d\nu, \mathbb{C}))} \\
& = \sup_{n \in \mathbb{N}_0} \left| \int_{-\pi}^{\pi} \frac{1}{B_T} \left[\int_{[-\sqrt{B_T}/2, \sqrt{B_T}/2]} W\left(\frac{\omega - \alpha}{B_T}\right) \frac{d\omega}{\sqrt{B_T}} \right] f_n^{(T)}(\alpha) d\alpha + \mathcal{O}(B_T^{-1}T^{-1}) \right| \\
& \geq g(T) = \mathcal{O}(B_T^{-1/2-l_\alpha}), \quad T \rightarrow \infty, \tag{79}
\end{aligned}$$

where $\mathcal{L}(L^2(\mathbb{M}_d, d\nu, \mathbb{C}))$ denotes the space of bounded linear operators on $L^2(\mathbb{M}_d, d\nu, \mathbb{C})$.

C.2 Proof of Theorem 4.2

Proof. From Lemmas 3.1 and 3.3, applying trace formula, for T sufficiently large,

$$\begin{aligned}
& \int_{-\pi}^{\pi} E_{H_1} \left\| \widehat{\mathcal{F}}_\omega^{(T)} - E_{H_1}[\widehat{\mathcal{F}}_\omega^{(T)}] \right\|_{\mathcal{S}(L^2(\mathbb{M}_d, d\nu, \mathbb{C}))}^2 d\omega \\
& \leq \frac{2\pi}{TB_T} \int_{-\pi}^{\pi} \sum_{n, h \in \mathbb{N}_0} \sum_{j=1}^{\Gamma(n, d)} \sum_{l=1}^{\Gamma(h, d)} \left| \int_{-\pi}^{\pi} \frac{1}{\sqrt{B_T}} W\left(\frac{\omega - \alpha}{B_T}\right) \frac{1}{\sqrt{B_T}} W\left(\frac{\omega - \alpha}{B_T}\right) \right. \\
& \quad \times f_n(\alpha) f_h(\alpha) d\alpha \Big| d\omega \\
& + \frac{2\pi}{TB_T} \int_{-\pi}^{\pi} \sum_{n, h \in \mathbb{N}_0} \sum_{j=1}^{\Gamma(n, d)} \sum_{l=1}^{\Gamma(h, d)} \left| \int_{-\pi}^{\pi} \frac{1}{\sqrt{B_T}} W\left(\frac{\omega - \alpha}{B_T}\right) \frac{1}{\sqrt{B_T}} W\left(\frac{\omega + \alpha}{B_T}\right) \right. \\
& \quad \times f_n(\alpha) f_h(\alpha) d\alpha \Big| d\omega \\
& + \mathcal{O}(B_T^{-2}T^{-2}) + \mathcal{O}(T^{-1}) \\
& \simeq \frac{2\pi}{TB_T} \int_{-\pi}^{\pi} \sum_{n, h \in \mathbb{N}_0} \sum_{j=1}^{\Gamma(n, d)} \sum_{l=1}^{\Gamma(h, d)} \left| \int_{-\pi}^{\pi} \delta_T(\omega - \alpha) f_n(\alpha) f_h(\alpha) d\alpha \right| d\omega \\
& + \frac{2\pi}{TB_T} \int_{-\pi}^{\pi} \sum_{n, h \in \mathbb{N}_0} \sum_{j=1}^{\Gamma(n, d)} \sum_{l=1}^{\Gamma(h, d)} \left| \int_{-\pi}^{\pi} \delta_T(\omega - \alpha) f_n(\alpha) f_h(\alpha) d\alpha \right| d\omega \\
& + \mathcal{O}(B_T^{-2}T^{-2}) + \mathcal{O}(T^{-1}) \\
& \simeq \frac{2\pi}{TB_T} \sum_{n, h \in \mathbb{N}_0} \sum_{j=1}^{\Gamma(n, d)} \sum_{l=1}^{\Gamma(h, d)} 2 \int_{[-\pi, \pi]} f_n(\omega) f_h(\omega) d\omega + \mathcal{O}(B_T^{-2}T^{-2}) + \mathcal{O}(T^{-1}) \\
& = h(T) = \mathcal{O}(B_T^{-1}T^{-1}), \quad T \rightarrow \infty, \tag{80}
\end{aligned}$$

where, as before, $a_T \simeq b_T$ means that the two sequences $\{a_T, T > 0\}$ and $\{b_T, T > 0\}$ have the same limit as $T \rightarrow \infty$.

Note that, under H_1 , equation (80) follows from condition

$$\int_{[-\pi, \pi]} \|\mathcal{M}_\omega\|_{L^1(L^2(\mathbb{M}_d, d\nu, \mathbb{C}))}^2 |\omega|^{-2L_\alpha} d\omega < \infty,$$

since

$$\begin{aligned} & \sum_{n, h \in \mathbb{N}_0} \sum_{j=1}^{\Gamma(n, d)} \sum_{l=1}^{\Gamma(h, d)} \int_{[-\pi, \pi]} f_n(\omega) f_h(\omega) d\omega \\ & \leq \sum_{n, h \in \mathbb{N}_0} \sum_{j=1}^{\Gamma(n, d)} \sum_{l=1}^{\Gamma(h, d)} \int_{[-\pi, \pi]} M_n(\omega) M_h(\omega) |\omega|^{-2L_\alpha} d\omega \\ & = \int_{[-\pi, \pi]} \|\mathcal{M}_\omega\|_{L^1(L^2(\mathbb{M}_d, d\nu, \mathbb{C}))}^2 |\omega|^{-2L_\alpha} d\omega = \mathcal{O}(1). \end{aligned}$$

C.3 Proof of Corollary 4.3

Proof. Applying triangle and Jensen inequalities, we obtain from Corollary 3.2 and Theorem 4.2,

$$\begin{aligned} & \left\| \int_{-\pi}^{\pi} E_{H_1} \left[\widehat{\mathcal{F}}_\omega^{(T)} - \int_{-\pi}^{\pi} W(\xi) \mathcal{F}_{\omega - B_T \xi} d\xi \right] d\omega \right\|_{\mathcal{S}(L^2(\mathbb{M}_d, d\nu, \mathbb{C}))} \\ & \leq \left\| \int_{-\pi}^{\pi} E_{H_1} \left[\widehat{\mathcal{F}}_\omega^{(T)} - E_{H_1} \left[\widehat{\mathcal{F}}_\omega^{(T)} \right] \right] d\omega \right\|_{\mathcal{S}(L^2(\mathbb{M}_d, d\nu, \mathbb{C}))} \\ & \quad + \left\| \int_{-\pi}^{\pi} \left[E_{H_1} \left[\widehat{\mathcal{F}}_\omega^{(T)} \right] - \int_{-\pi}^{\pi} W(\xi) \mathcal{F}_{\omega - B_T \xi} d\xi \right] d\omega \right\|_{\mathcal{S}(L^2(\mathbb{M}_d, d\nu, \mathbb{C}))} \\ & \leq \left[\int_{-\pi}^{\pi} E_{H_1} \left\| \widehat{\mathcal{F}}_\omega^{(T)} - E_{H_1} \left[\widehat{\mathcal{F}}_\omega^{(T)} \right] \right\|_{\mathcal{S}(L^2(\mathbb{M}_d, d\nu, \mathbb{C}))}^2 d\omega \right]^{1/2} \\ & \quad + \left\| \int_{-\pi}^{\pi} \left[E_{H_1} \left[\widehat{\mathcal{F}}_\omega^{(T)} \right] - \int_{-\pi}^{\pi} W(\xi) \mathcal{F}_{\omega - B_T \xi} d\xi \right] d\omega \right\|_{\mathcal{S}(L^2(\mathbb{M}_d, d\nu, \mathbb{C}))} \\ & = \mathcal{O}(T^{-1/2} B_T^{-1/2}), \quad T \rightarrow \infty. \end{aligned} \tag{81}$$

C.4 Proof of Theorem 4.4

Proof. The proof of this result shares some ideas with the proof of Theorem 2 of [15], formulated in the time domain for real-valued time series. Specifically,

the test statistic operator \mathcal{S}_{B_T} is rewritten as

$$\begin{aligned} \mathcal{S}_{B_T} &= \sqrt{B_T T} \int_{[-\sqrt{B_T}/2, \sqrt{B_T}/2]} E_{H_1} \left[\widehat{\mathcal{F}}_\omega^{(T)} \right] \frac{d\omega}{\sqrt{B_T}} \\ &\circ \left[\mathbb{I}_{L^2(\mathbb{M}_d, d\nu, \mathbb{C})} + \left[\int_{[-\sqrt{B_T}/2, \sqrt{B_T}/2]} \left(\widehat{\mathcal{F}}_\omega^{(T)} - E_{H_1} \left[\widehat{\mathcal{F}}_\omega^{(T)} \right] \right) \frac{d\omega}{\sqrt{B_T}} \right] \right. \\ &\quad \left. \circ \left[\int_{[-\sqrt{B_T}/2, \sqrt{B_T}/2]} E_{H_1} \left[\widehat{\mathcal{F}}_\omega^{(T)} \right] \frac{d\omega}{\sqrt{B_T}} \right]^{-1} \right], \end{aligned} \quad (82)$$

where \circ means the composition of operators, $\mathbb{I}_{L^2(\mathbb{M}_d, d\nu, \mathbb{C})}$ denotes the identity operator on the space $L^2(\mathbb{M}_d, d\nu, \mathbb{C})$, and $\left[\int_{[-\sqrt{B_T}/2, \sqrt{B_T}/2]} E_{H_1} \left[\widehat{\mathcal{F}}_\omega^{(T)} \right] \frac{d\omega}{\sqrt{B_T}} \right]^{-1}$ is the inverse of operator $\int_{[-\sqrt{B_T}/2, \sqrt{B_T}/2]} E_{H_1} \left[\widehat{\mathcal{F}}_\omega^{(T)} \right] \frac{d\omega}{\sqrt{B_T}}$.

Our strategy in the proof of this result consists of first proving, under H_1 , the divergence, in the norm of the space $\mathcal{S}(L^2(\mathbb{M}_d, d\nu, \mathbb{C}))$, of operator $\sqrt{B_T T} \int_{[-\sqrt{B_T}/2, \sqrt{B_T}/2]} E_{H_1} \left[\widehat{\mathcal{F}}_\omega^{(T)} \right] \frac{d\omega}{\sqrt{B_T}}$. Then, under the conditions of Theorem 4.2, we derive the convergence to zero, as $T \rightarrow \infty$, of random operator

$$\begin{aligned} &\left[\int_{[-\sqrt{B_T}/2, \sqrt{B_T}/2]} \left[\widehat{\mathcal{F}}_\omega^{(T)} - E_{H_1} \left[\widehat{\mathcal{F}}_\omega^{(T)} \right] \right] \frac{d\omega}{\sqrt{B_T}} \right] \\ &\quad \circ \left[\int_{[-\sqrt{B_T}/2, \sqrt{B_T}/2]} E_{H_1} \left[\widehat{\mathcal{F}}_\omega^{(T)} \right] \frac{d\omega}{\sqrt{B_T}} \right]^{-1}, \end{aligned} \quad (83)$$

in the space $\mathcal{L}_{\mathcal{S}(L^2(\mathbb{M}_d, d\nu, \mathbb{C}))}^2(\Omega, \mathcal{A}, P)$, which holds with a suitable rate under $l_\alpha > 1/4$ and $B_T = T^{-\beta}$, $\beta \in (0, 1)$, allowing the application of Borell Cantelli Lemma to ensure almost surely convergence. Specifically, from Proposition 4.1, as $T \rightarrow \infty$,

$$\begin{aligned} &\left\| \sqrt{B_T T} \int_{[-\sqrt{B_T}/2, \sqrt{B_T}/2]} E_{H_1} \left[\widehat{\mathcal{F}}_\omega^{(T)} \right] \frac{d\omega}{\sqrt{B_T}} \right\|_{\mathcal{S}(L^2(\mathbb{M}_d, d\nu, \mathbb{C}))} \\ &\quad \geq g(T) = \mathcal{O}(T^{1/2} B_T^{-l_\alpha}). \end{aligned} \quad (84)$$

For the random operator in (83), the following inequality holds:

$$\begin{aligned}
& E_{H_1} \left\| \int_{[-\sqrt{B_T}/2, \sqrt{B_T}/2]} \left[\widehat{\mathcal{F}}_\omega^{(T)} - E_{H_1} \left[\widehat{\mathcal{F}}_\omega^{(T)} \right] \right] \frac{d\omega}{\sqrt{B_T}} \right. \\
& \quad \left. \circ \left[\int_{[-\sqrt{B_T}/2, \sqrt{B_T}/2]} E_{H_1} \left[\widehat{\mathcal{F}}_\omega^{(T)} \right] \frac{d\omega}{\sqrt{B_T}} \right]^{-1} \right\|_{\mathcal{S}(L^2(\mathbb{M}_d, d\nu, \mathbb{C}))}^2 \\
& \leq \left\| \left[\int_{[-\sqrt{B_T}/2, \sqrt{B_T}/2]} E_{H_1} \left[\widehat{\mathcal{F}}_\omega^{(T)} \right] \frac{d\omega}{\sqrt{B_T}} \right]^{-1} \right\|_{\mathcal{L}(L^2(\mathbb{M}_d, d\nu, \mathbb{C}))}^2 \\
& \quad \times E_{H_1} \left\| \int_{[-\sqrt{B_T}/2, \sqrt{B_T}/2]} \left[\widehat{\mathcal{F}}_\omega^{(T)} - E_{H_1} \left[\widehat{\mathcal{F}}_\omega^{(T)} \right] \right] \frac{d\omega}{\sqrt{B_T}} \right\|_{\mathcal{S}(L^2(\mathbb{M}_d, d\nu, \mathbb{C}))}^2 \quad (85)
\end{aligned}$$

From equation (79), as $T \rightarrow \infty$,

$$\left\| \left[\int_{[-\sqrt{B_T}/2, \sqrt{B_T}/2]} E_{H_1} \left[\widehat{\mathcal{F}}_\omega^{(T)} \right] \frac{d\omega}{\sqrt{B_T}} \right]^{-1} \right\|_{\mathcal{L}(L^2(\mathbb{M}_d, d\nu, \mathbb{C}))}^2 \leq b(T) = \mathcal{O}(B_T^{2l_\alpha+1}), \quad (86)$$

and, from Theorem 4.2,

$$\begin{aligned}
& \int_{[-\sqrt{B_T}/2, \sqrt{B_T}/2]} \text{Var}_{H_1} \left(\widehat{\mathcal{F}}_\omega^{(T)} \right) \frac{d\omega}{\sqrt{B_T}} \\
& \leq \int_{[-\pi, \pi]} \text{Var}_{H_1} \left(\widehat{\mathcal{F}}_\omega^{(T)} \right) \frac{d\omega}{\sqrt{B_T}} \leq u(T) = \mathcal{O}(T^{-1} B_T^{-1-1/2}), \quad T \rightarrow \infty. \quad (87)
\end{aligned}$$

For each $T \geq 2$, applying Jensen inequality, in terms of the uniform probability measure on the interval $[-\sqrt{B_T}/2, \sqrt{B_T}/2]$,

$$\begin{aligned}
& E_{H_1} \left\| \int_{[-\sqrt{B_T}/2, \sqrt{B_T}/2]} \left[\widehat{\mathcal{F}}_\omega^{(T)} - E_{H_1} \left[\widehat{\mathcal{F}}_\omega^{(T)} \right] \right] \frac{d\omega}{\sqrt{B_T}} \right\|_{\mathcal{S}(L^2(\mathbb{M}_d, d\nu, \mathbb{C}))}^2 \\
& = \left\| \int_{[-\sqrt{B_T}/2, \sqrt{B_T}/2]} \left[\widehat{\mathcal{F}}_\omega^{(T)} - E_{H_1} \left[\widehat{\mathcal{F}}_\omega^{(T)} \right] \right] \frac{d\omega}{\sqrt{B_T}} \right\|_{\mathcal{L}^2(\mathcal{S}(L^2(\mathbb{M}_d, d\nu, \mathbb{C}))^{(\Omega, \mathcal{A}, P)})}^2 \\
& = \varphi_{H_1} \left(E_{\mathcal{U}([- \sqrt{B_T}/2, \sqrt{B_T}/2])} \left[\widehat{\mathcal{F}}_\omega^{(T)} - E_{H_1} \left[\widehat{\mathcal{F}}_\omega^{(T)} \right] \right] \right) \\
& \leq E_{\mathcal{U}([- \sqrt{B_T}/2, \sqrt{B_T}/2])} \left[\varphi_{H_1} \left(\left[\widehat{\mathcal{F}}_\omega^{(T)} - E_{H_1} \left[\widehat{\mathcal{F}}_\omega^{(T)} \right] \right] \right) \right] \\
& = \int_{[-\sqrt{B_T}/2, \sqrt{B_T}/2]} E_{H_1} \left\| \widehat{\mathcal{F}}_\omega^{(T)} - E_{H_1} \left[\widehat{\mathcal{F}}_\omega^{(T)} \right] \right\|_{\mathcal{S}(L^2(\mathbb{M}_d, d\nu, \mathbb{C}))}^2 \frac{d\omega}{\sqrt{B_T}}, \quad (88)
\end{aligned}$$

where $E_{\mathcal{U}([- \sqrt{B_T}/2, \sqrt{B_T}/2])}$ denotes expectation under the uniform probability measure on the interval $[- \sqrt{B_T}/2, \sqrt{B_T}/2]$, and $\varphi_{H_1}(\cdot) = \|\cdot\|_{\mathcal{L}^2_{\mathcal{S}(L^2(\mathbb{M}_d, d\nu, \mathbb{C}))}(\Omega, \mathcal{A}, P)}^2 = E_{H_1} \|\cdot\|_{\mathcal{S}(L^2(\mathbb{M}_d, d\nu, \mathbb{C}))}^2$ is a convex function. Thus, from equations (85)–(88),

$$\begin{aligned} E_{H_1} \left\| \int_{[- \sqrt{B_T}/2, \sqrt{B_T}/2]} \left[\widehat{\mathcal{F}}_\omega^{(T)} - E_{H_1} \left[\widehat{\mathcal{F}}_\omega^{(T)} \right] \right] \frac{d\omega}{\sqrt{B_T}} \right. \\ \left. \circ \left[\int_{[- \sqrt{B_T}/2, \sqrt{B_T}/2]} E_{H_1} \left[\widehat{\mathcal{F}}_\omega^{(T)} \right] \frac{d\omega}{\sqrt{B_T}} \right]^{-1} \right\|_{\mathcal{S}(L^2(\mathbb{M}_d, d\nu, \mathbb{C}))}^2 \\ \leq h(T) = \mathcal{O}(T^{-1} B_T^{2l_\alpha - 1/2}), \quad T \rightarrow \infty. \end{aligned} \quad (89)$$

From equation (89), applying Chebyshev's inequality,

$$\begin{aligned} P \left[\left\| \int_{[- \sqrt{B_T}/2, \sqrt{B_T}/2]} \left[\widehat{\mathcal{F}}_\omega^{(T)} - E_{H_1} \left[\widehat{\mathcal{F}}_\omega^{(T)} \right] \right] \frac{d\omega}{\sqrt{B_T}} \right. \right. \\ \left. \left. \circ \left[\int_{[- \sqrt{B_T}/2, \sqrt{B_T}/2]} E_{H_1} \left[\widehat{\mathcal{F}}_\omega^{(T)} \right] \frac{d\omega}{\sqrt{B_T}} \right]^{-1} \right\|_{\mathcal{S}(L^2(\mathbb{M}_d, d\nu, \mathbb{C}))} > \varepsilon \right] \\ \leq E_{H_1} \left\| \int_{[- \sqrt{B_T}/2, \sqrt{B_T}/2]} \left[\widehat{\mathcal{F}}_\omega^{(T)} - E_{H_1} \left[\widehat{\mathcal{F}}_\omega^{(T)} \right] \right] \frac{d\omega}{\sqrt{B_T}} \right. \\ \left. \circ \left[\int_{[- \sqrt{B_T}/2, \sqrt{B_T}/2]} E_{H_1} \left[\widehat{\mathcal{F}}_\omega^{(T)} \right] \frac{d\omega}{\sqrt{B_T}} \right]^{-1} \right\|_{\mathcal{S}(L^2(\mathbb{M}_d, d\nu, \mathbb{C}))}^2 / \varepsilon^2 \\ \leq h(T) / \varepsilon^2 = \mathcal{O}(T^{-1} B_T^{2l_\alpha - 1/2}). \end{aligned} \quad (90)$$

Since $l_\alpha > 1/4$, hence, $2l_\alpha - 1/2 = \rho > 0$, and, for $B_T = T^{-\beta}$, $T^{-1} B_T^{2l_\alpha - 1/2} = T^{-1-\beta\rho}$, with $\beta \in (0, 1)$, and $\rho \in (0, 1/2)$. From equation (90), Borel–Cantelli lemma then leads to, as $T \rightarrow \infty$,

$$\begin{aligned} \left\| \int_{[- \sqrt{B_T}/2, \sqrt{B_T}/2]} \left[\widehat{\mathcal{F}}_\omega^{(T)} - E_{H_1} \left[\widehat{\mathcal{F}}_\omega^{(T)} \right] \right] \frac{d\omega}{\sqrt{B_T}} \right. \\ \left. \circ \left[\int_{[- \sqrt{B_T}/2, \sqrt{B_T}/2]} E_{H_1} \left[\widehat{\mathcal{F}}_\omega^{(T)} \right] \frac{d\omega}{\sqrt{B_T}} \right]^{-1} \right\|_{\mathcal{S}(L^2(\mathbb{M}_d, d\nu, \mathbb{C}))} \rightarrow_{a.s.} 0. \end{aligned} \quad (91)$$

The a.s. divergence of $\|\mathcal{S}_{B_T}\|_{\mathcal{S}(L^2(\mathbb{M}_d, d\nu, \mathbb{C}))}$, as $T \rightarrow \infty$, follows from equations (82), (84) and (91).

C.5 Proof of Lemma 4.6

Proof. For $\omega \in (-\pi, \pi) \setminus \{0\}$, consider a Gaussian random element $\widehat{\mathcal{F}}_\omega$ in $\mathcal{S}(L^2(\mathbb{M}_d, d\nu, \mathbb{C}))$, with kernel \widehat{f}_ω satisfying (45). Hence, from (47),

$$\begin{aligned} & \frac{1}{2\pi \|W\|_{L^2(\mathbb{R})}^2} E \left[\widehat{f}_\omega \otimes \widehat{f}_\omega \right] (\tau_1, \sigma_1, \tau_2, \sigma_2) \\ &= \sum_{n,h \in \mathbb{N}_0} \sum_{j=1}^{\Gamma(n,d)} \sum_{l=1}^{\Gamma(h,d)} f_n(\omega) f_h(\omega) S_{n,j}^d(\tau_1) \overline{S_{h,l}^d(\sigma_1) S_{n,j}^d(\tau_2) S_{h,l}^d(\sigma_2)}, \end{aligned} \quad (92)$$

for every $(\tau_i, \sigma_i) \in \mathbb{M}_d^2$, $i = 1, 2$, $\omega \in (-\pi, \pi) \setminus \{0\}$. Thus, the diagonal coefficients $\{\lambda_{n,h}(\omega), n, h \in \mathbb{N}_0\} = \{f_n(\omega) f_h(\omega), n, h \in \mathbb{N}_0\}$ define the eigenvalues of the autocovariance operator (92). Since \mathbb{M}_d^2 is a compact set, and $\mathcal{R}_{\widehat{\mathcal{F}}_\omega, \widehat{\mathcal{F}}_\omega}$ is a trace positive semidefinite self-adjoint operator under H_0 , the orthogonal expansion

$$\frac{1}{\sqrt{2\pi} \|W\|_{L^2(\mathbb{R})}} \widehat{f}_\omega(\tau, \sigma) = \sum_{n,h \in \mathbb{N}_0} \sum_{j=1}^{\Gamma(n,d)} \sum_{l=1}^{\Gamma(h,d)} \sqrt{f_n(\omega) f_h(\omega)} Y_{n,j,h,l}(\omega) S_{n,j}^d(\tau) \overline{S_{h,l}^d(\sigma)} \quad (93)$$

holds in the space $\mathcal{L}_{\mathcal{S}(L^2(\mathbb{M}_d, d\nu; \mathbb{C}))}^2(\Omega, \mathcal{A}, \mathcal{P})$. The random Fourier coefficients are given by

$$\begin{aligned} Y_{n,j,h,l}(\omega) &= \frac{(\sqrt{2\pi} \|W\|_{L^2(\mathbb{R})})^{-1}}{\sqrt{f_n(\omega) f_h(\omega)}} \int_{\mathbb{M}_d^2} \widehat{f}_\omega(\tau, \sigma) \overline{S_{n,j}^d(\tau) S_{h,l}^d(\sigma)} d\nu(\sigma) d\nu(\tau), \\ & j = 1, \dots, \Gamma(n, d), \quad l = 1, \dots, \Gamma(h, d), \quad n, h \in \mathbb{N}_0, \quad \omega \in (-\pi, \pi) \setminus \{0\}. \end{aligned} \quad (94)$$

D Figures of Sections 5.2 and 5.3

This Appendix includes the figures illustrating the numerical results of Sections 5.2 and 5.3.

D.1 Examples

This section contains the figures displayed in Examples 1–4 analyzed in Sections 5.2–5.3. Specifically, it provides the generated realizations of multifractionally integrated SPHARMA (1,1) processes, the eigenvalues of LRD operator \mathcal{A} defining the multifractional integration operators, and the sample values of \mathcal{S}_{B_T} projected into $\mathcal{H}_n \otimes \mathcal{H}_n$, $n = 1, \dots, 8$, for large values of T .

D.1.1 Example 1

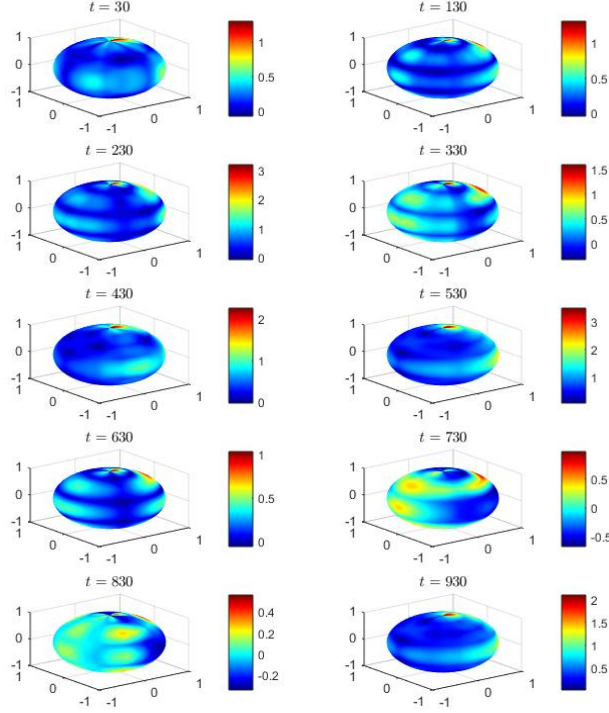


Figure 5: *Example 1.* One sample realization at times $t = 30, 130, 230, 330, 430, 530, 630, 730, 830, 930$ of multifractionally integrated SPHARMA(1,1) process projected into $\bigoplus_{n=1}^8 \mathcal{H}_n$

Figure 5 displays one sample realization of the generated multifractionally integrated SPHARMA (1,1) process projected into $\bigoplus_{n=1}^8 \mathcal{H}_n$, with $\lambda_n(\varphi_1) = 0.7 \left(\frac{n+1}{n}\right)^{-3/2}$ and $\lambda_n(\psi_1) = (0.4) \left(\frac{n+1}{n}\right)^{-5/1.95}$, $n \in \mathbb{N}_0$. The eigenvalues $\alpha(n)$, $n = 1, 2, 3, 4, 5, 6, 7, 8$, of LRD operator \mathcal{A} are plotted at the left-hand side of Figure 6, being $L_\alpha = 0.4733$, and $l_\alpha = 0.2678$, and $\alpha(n) = l_\alpha = 0.2678$, $n \geq 9$. The a.s. divergence in the Hilbert–Schmidt operator norm of \mathcal{S}_{B_T} , for $B_T = T^{-1/4}$, projected into $\mathcal{H}_n \otimes \mathcal{H}_n$, $n = 1, \dots, 8$, is illustrated in the three plots at the right-hand side of Figure 6.

D.1.2 Example 2

Figure 7 displays one sample realization of the generated multifractionally integrated SPHARMA (1,1) process projected into $\bigoplus_{n=1}^8 \mathcal{H}_n$, with $\lambda_n(\varphi_1) =$

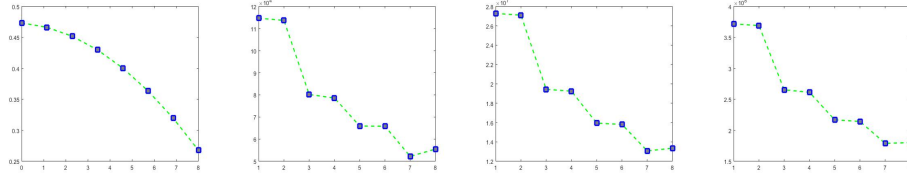


Figure 6: *Example 1.* Eigenvalues $\alpha(n)$, $n = 1, 2, 3, 4, 5, 6, 7, 8$, of LRD operator \mathcal{A} , $L_\alpha = 0.4733$, and $l_\alpha = 0.2678$ (plot at the left-hand side). Sample values of the test operator statistics \mathcal{S}_{B_T} , $B_T = T^{-1/4}$, projected into $\mathcal{H}_n \otimes \mathcal{H}_n$, $n = 1, \dots, 8$ for functional sample sizes $T = 1000, 10000, 30000$ (three plots at the right-hand side)

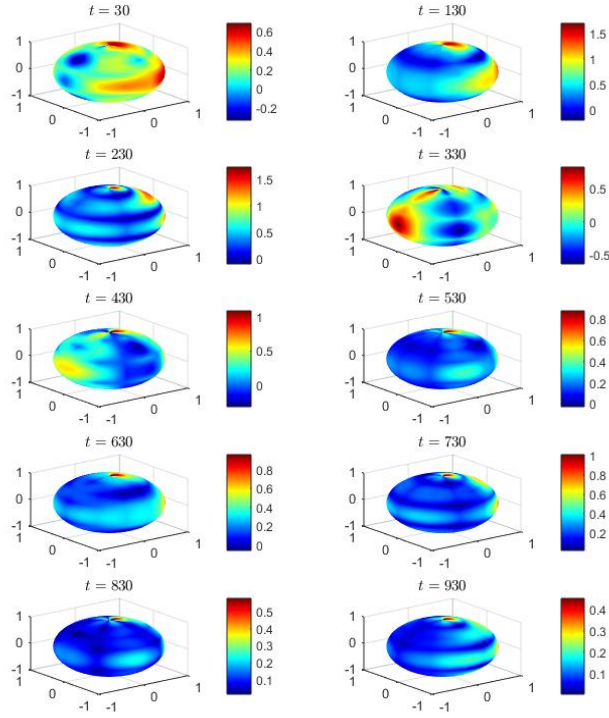


Figure 7: *Example 2.* One sample realization at times $t = 30, 130, 230, 330, 430, 530, 630, 730, 830, 930$ of multifractionally integrated SPHARMA(1,1) process projected into $\bigoplus_{n=1}^8 \mathcal{H}_n$

$0.7 \left(\frac{n+1}{n}\right)^{-3/2}$ and $\lambda_n(\psi_1) = (0.4) \left(\frac{n+1}{n}\right)^{-5/1.95}$, $n \in \mathbb{N}_0$. The eigenvalues $\alpha(n)$, $n = 1, 2, 3, 4, 5, 6, 7, 8$, of LRD operator \mathcal{A} are plotted at the left-hand side of Figure 8, being $L_\alpha = 0.3327$, and $l_\alpha = 0.2550$, with $\alpha(n) = l_\alpha = 0.2550$, $n \geq 9$. The a.s. divergence in the Hilbert–Schmidt operator norm of \mathcal{S}_{B_T} , for

$B_T = T^{-1/4}$, projected into $\mathcal{H}_n \otimes \mathcal{H}_n$, $n = 1, \dots, 8$, is illustrated in the three plots at the right-hand side of Figure 8.

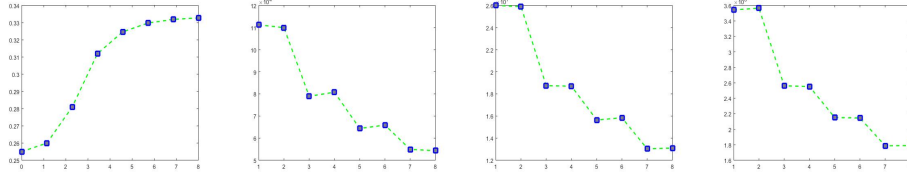


Figure 8: *Example 2.* Eigenvalues $\alpha(n)$, $n = 1, 2, 3, 4, 5, 6, 7, 8$, of LRD operator \mathcal{A} , $L_\alpha = 0.3327$, and $l_\alpha = 0.2550$ (plot at the left-hand side). Sample values of the kernel of the test operator statistics \mathcal{S}_{B_T} , $B_T = T^{-1/4}$, projected into $\mathcal{H}_n \otimes \mathcal{H}_n$, $n = 1, \dots, 8$, for functional sample sizes $T = 1000, 10000, 30000$ (three plots at the right-hand side)

D.1.3 Example 3

Figure 9 displays one sample realization of the generated multifractionally integrated SPHARMA (1,1) process projected into $\bigoplus_{n=1}^8 \mathcal{H}_n$, with $\lambda_n(\varphi_1) = 0.7 \left(\frac{n+1}{n}\right)^{-3/2}$ and $\lambda_n(\psi_1) = (0.4) \left(\frac{n+1}{n}\right)^{-5/1.95}$, $n \in \mathbb{N}_0$. The eigenvalues $\alpha(n)$, $n = 1, 2, 3, 4, 5, 6, 7, 8$, of LRD operator \mathcal{A} are plotted at the left-hand side of Figure 10, being $L_\alpha = 0.4000$, and $l_\alpha = 0.2753 = \alpha(n)$, $n \geq 9$. The a.s. divergence in the Hilbert–Schmidt operator norm of \mathcal{S}_{B_T} , for $B_T = T^{-1/4}$, projected into $\mathcal{H}_n \otimes \mathcal{H}_n$, $n = 1, \dots, 8$, is illustrated in the three plots at the right-hand side of Figure 10.

D.1.4 Example 4

Figure 11 displays one sample realization of the generated multifractionally integrated SPHARMA (1,1) process projected into $\bigoplus_{n=1}^8 \mathcal{H}_n$, with $\lambda_n(\varphi_1) = 0.7 \left(\frac{n+1}{n}\right)^{-3/2}$ and $\lambda_n(\psi_1) = (0.4) \left(\frac{n+1}{n}\right)^{-5/1.95}$, $n \in \mathbb{N}_0$. Multifractional integration is given in terms of the eigenvalues $\alpha(n)$, $n = 1, 2, 3, 4, 5, 6, 7, 8$, of LRD operator \mathcal{A} , plotted at the left-hand side of Figure 12, being $L_\alpha = 0.9982$ and $l_\alpha = 0.3041$. The sample values of \mathcal{S}_{B_T} , for $B_T = T^{-1/4}$, projected into $\mathcal{H}_n \otimes \mathcal{H}_n$, $n = 1, \dots, 8$, are given in the three plots at the right-hand side of Figure 12.

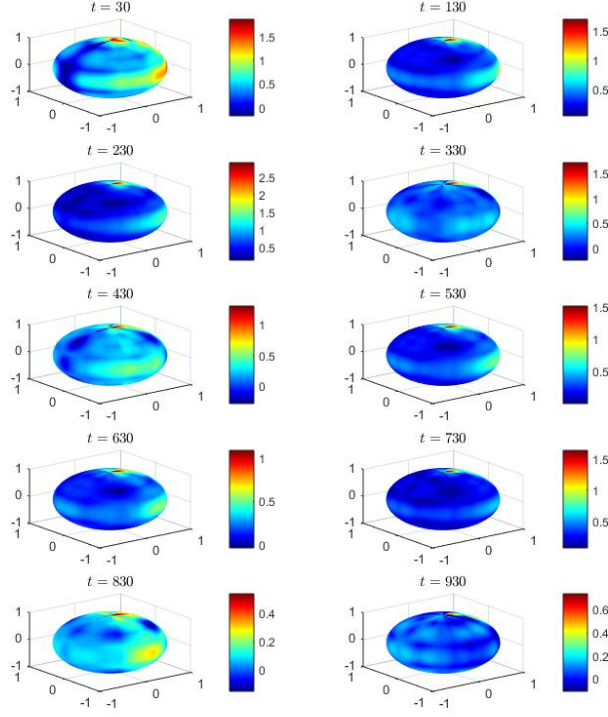


Figure 9: *Example 3.* One sample realization at times $t = 30, 130, 230, 330, 430, 530, 630, 730, 830, 930$ of multifractionally integrated SPHARMA(1,1) process projected into $\bigoplus_{n=1}^8 \mathcal{H}_n$

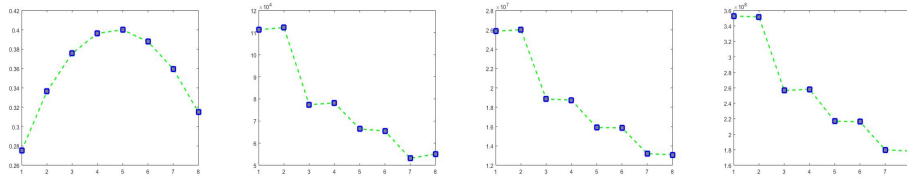


Figure 10: *Example 3.* Eigenvalues $\alpha(n)$, $n = 1, 2, 3, 4, 5, 6, 7, 8$, of the LRD operator \mathcal{A} , $L_\alpha = 0.4000$, and $l_\alpha = 0.2753$ (plot at the left-hand side). Sample values of the kernel of the test operator statistics \mathcal{S}_{B_T} , $B_T = T^{-1/4}$, projected into $\mathcal{H}_n \otimes \mathcal{H}_n$, $n = 1, \dots, 8$, for functional sample sizes $T = 1000, 10000, 30000$ (three plots at the right-hand side)

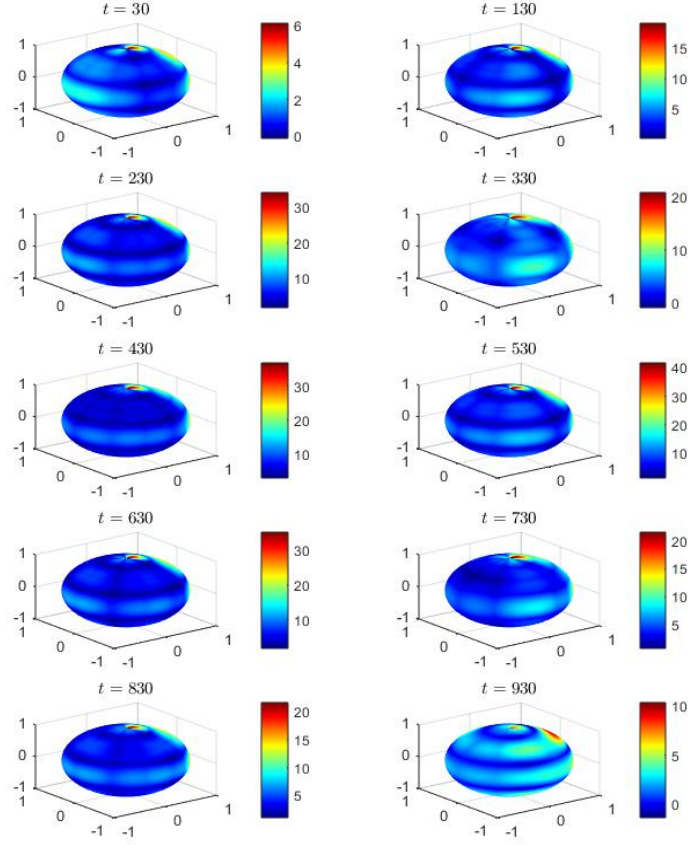


Figure 11: *Example 4.* One sample realization at times $t = 30, 130, 230, 330, 430, 530, 630, 730, 830, 930$ of multifractionally integrated SPHARMA(1,1) process projected into $\bigoplus_{n=1}^8 \mathcal{H}_n$

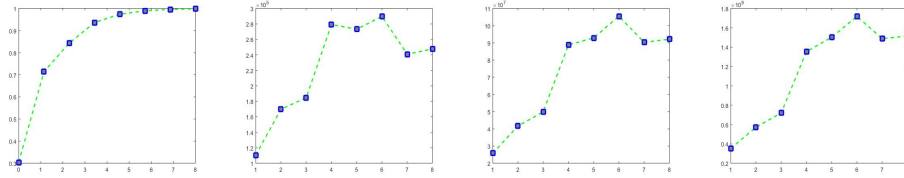


Figure 12: *Example 4.* Eigenvalues $\alpha(n)$, $n = 1, 2, 3, 4, 5, 6, 7, 8$, of LRD operator \mathcal{A} , $L_\alpha = 0.9982$ and $l_\alpha = 0.3041$ (plot at the left-hand side). Sample values of the kernel of the test operator statistics \mathcal{S}_{B_T} , for $B_T = T^{-1/4}$, projected into $\mathcal{H}_n \otimes \mathcal{H}_n$, $n = 1, \dots, 8$, for the functional sample sizes $T = 1000, 10000, 30000$ (three plots at the right-hand side)

References

- [1] BERAN, J. (2017). *Mathematical Foundations of Time Series Analysis*. Springer, Switzerland.
- [2] CAPONERA, A. (2021). SPHARMA approximations for stationary functional time series in the sphere. *Stat Infer Stoch Proc* **24** 609–634.
- [3] CAPONERA, A. and MARINUCCI, D. (2021). Asymptotics for spherical functional autoregressions. *Ann Stat* **49** 346–369.
- [4] CHARACIEJUS, V. and RÄCKAUSKAS, A. (2014). Operator self-similar processes and functional central limit theorems. *Stochastic Process Appl* **124** 2605–2627.
- [5] CUESTA-ALBERTOS, J.A., FRAIMAN, R. and RANSFORD, T. (2007). A sharp form of the Cramér–Wold theorem. *J Theoret Probab* **20** 201–209.
- [6] CUESTA-ALBERTOS, J. A., GARCÍA-PORTUGUÉS, E., FEBRERO-BANDE, M. and GONZÁLEZ-MANTEIGA, W. (2019). Goodness-of-fit tests for the functional linear model based on randomly projected empirical processes. *The Annals of Statistics* **47**, 439–467.
- [7] DA PRATO, G. and ZABCZYK, J. (2002). *Second Order Partial Differential Equations in Hilbert Spaces*. Cambridge, London.
- [8] DAUTRAY, R. and LIONS, J.L. (1985). *Mathematical Analysis and Numerical Methods for Science and Technology*. Volume **3**: *Spectral Theory and Applications*. Springer, New York.
- [9] DÜKER, M. (2018). Limit theorems for Hilbert space-valued linear processes under long range dependence. *Stochastic Processes and Their Applications* **128** 1439–1465.
- [10] DÜKER, M. (2020). Sample autocovariance operators of long-range dependent Hilbert space-valued linear processes. <https://www.researchgate.net/publication/344364182>.
- [11] DUQUE, J. C., CARONES, A., MARINUCCI, D., MIGLIACCIO, M. and VITTORIO, N. (2024). Minkowski functionals in $SO(3)$ for the spin-2 CMB polarisation field. *Journal of Cosmology and Astroparticle Physics*. <https://doi.org/10.1088/1475-7516/2024/01/039>.
- [12] GELFAND, I. M. and VILENKIN, N. Y. (1964). *Generalized Functions*, Vol. 4. Academic Press, New York.

- [13] GINÉ, M. (1975). The addition formula for the eigenfunctions of the Laplacian. *Advances in Mathematics* **18** 102–107.
- [14] HELGASON, S. (1959). Differential operators on homogeneous spaces. *Acta Math* **102**, 239–299.
- [15] HARRIS, D., MCCABE, B. and LEYBOURNE, S. (2008). Testing for long memory. *Econometric Theory* **24** 143–175.
- [16] LI, D., ROBINSON, P.M. and SHANG, H.L. (2019). Long-range dependent curve time series. *Journal of the American Statistical Association* **115** 957–971.
- [17] MA, C. and MALYARENKO, A. (2020). Time varying isotropic vector random fields on compact two points homogeneous spaces. *J Theor Probab* **33** 319–339.
- [18] MARINUCCI, D. (2004). Testing for non-gaussianity on cosmic microwave background radiation: A review. *Statistical Science* **19** 294–307.
- [19] MARINUCCI, D. and PECCATI, G. (2011). *Random fields on the Sphere. Representation, Limit Theorems and Cosmological Applications*. Mathematical Society Lecture Note Series 389. Cambridge University Press, London.
- [20] MARINUCCI, D., ROSSI, M. and VIDOTTO, A. (2020). Non-universal fluctuations of the empirical measure for isotropic stationary fields on $\mathbb{S}^2 \times \mathbb{R}$. *Ann Appl Probab* **31** 2311–2349.
- [21] MARINUCCI, D., ROSSI, M. and WIGMAN, I. (2020). The asymptotic equivalence of the sample trispectrum and the nodal length for random spherical harmonics. *Ann Inst Henri Poincaré Probab Stat* **56** 374–390.
- [22] OVALLE–MUÑOZ, D. P. and RUIZ–MEDINA, M. D. (2024a). LRD spectral analysis of multifractional functional time series on manifolds. *TEST* **33** 564–588.
- [23] OVALLE–MUÑOZ, D. P. and RUIZ–MEDINA, M. D. (2024b). Climate change analysis from LRD manifold functional regression. arXiv.5699574.
- [24] PANARETOS, V. M. and TAVAKOLI, S. (2013a). Fourier analysis of stationary time series in function space. *Ann Statist* **41** 568–603.
- [25] PANARETOS, V. M. and TAVAKOLI, S. (2013b). Cramér–Karhunen–Loève representation and harmonic principal component analysis of functional time series. *Stochastic Process and their Applications* **123** 2779–2807.

- [26] PHAM, T. and PANARETOS, V. (2018). Methodology and convergence rates for functional time series regression. *Statistica Sinica* **28** 2521–2539.
- [27] RACKAUSKAS, A. and SUQUET, CH. (2010). On limit theorems for Banach-space-valued linear processes. *Lithuanian Mathematical J* **50** 71–87.
- [28] RACKAUSKAS, A. and SUQUET, CH. (2011). Operator fractional brownian motion as limit of polygonal lines processes in Hilbert space. *Stochastics and Dynamics* **11** 49–70.
- [29] RAMM, A.G. (2005). *Random Fields Estimation*. Longman Scientific & Technical, England.
- [30] RUBÍN, T. and PANARETOS, V. M. (2020a). Functional lagged regression with sparse noisy observations. *Journal of Time Series Analysis* **41** 858–882.
- [31] RUBÍN, T. and PANARETOS, V. M. (2020b). Spectral simulation of functional time series. *arXiv preprint arXiv:2007.08458*.
- [32] RUIZ-MEDINA, M. D. (2022). Spectral analysis of long range dependence functional time series. *Fractional Calculus and Applied Analysis* **25** 1426–1458.
- [33] SHAH, I., MUBASSIR, P., ALI, S. and ALBALAWI, O. (2024). A functional autoregressive approach for modeling and forecasting short-term air temperature. *Environ Sci* **12** <https://doi.org/10.3389/fenvs.2024.1411237>.
- [34] TAVAKOLI, S. (2014). *Fourier Analysis of Functional Time Series with Applications to DNA Dynamics*. Ph.D. dissertation, EPFL. Available at <http://dx.doi.org/10.5075/epfl-thesis-6320>.
- [35] TAVAKOLI, S. and PANARETOS, V. M. (2016). Detecting and localizing differences in functional time series dynamics: a case study in molecular biophysics. *Journal of the American Statistical Association* **111** 1020–1035.
- [36] TIRELLI, I., MENDEZ, M. A., IANIRO, A. and DISCETTI, S. (2024). A meshless method to compute the proper orthogonal decomposition and its variants from scattered data. *ArXiv* 2407.03173.
- [37] WU, Y., HUANG, CH. and SRIVASTAVA, A. (2024). Shape based functional data analysis. *TEST* **33** 1–47.
- [38] YARGER, D., STOEV, S. and HSING, T. (2022). A functional-data approach to the Argo data. *Ann Appl Stat* **16** 216–246.

- [39] ZHOU, H., LI, L. and ZHU, H. (2013). Tensor regression with applications in neuroimaging data analysis. *J Am Stat Assoc* **108** 540–552.
- [40] ZHOU, H., WEI, D. and YAO, F. (2024). Theory of functional principal component analysis for discretely observed data. ArXiv: 2209.08768v4.
- [41] ZHU, H., CHEN, Y., IBRAHIM, J. G., LI, Y., HALL, C. and LIN, W. (2009). Intrinsic regression models for positive-definite matrices with applications to diffusion tensor imaging. *J Am Stat Assoc* **104** 1203–1212.